

## RESEARCH ARTICLE

# FliL and its paralog MotF have distinct roles in the stator activity of the *Sinorhizobium meliloti* flagellar motor

Richard C. Sobe<sup>1</sup> | Crystal Gilbert<sup>1</sup> | Lam Vo<sup>2</sup> | Gladys Alexandre<sup>2</sup> | Birgit E. Scharf<sup>1</sup>

<sup>1</sup>Department of Biological Sciences, Life Sciences I, Virginia Tech, Blacksburg, Virginia, USA

<sup>2</sup>Department of Biochemistry and Cell and Molecular Biology, University of Tennessee at Knoxville, Knoxville, Tennessee, USA

## Correspondence

Birgit E. Scharf, Department of Biological Sciences, Life Sciences I, Virginia Tech, Blacksburg, VA 24061, USA.  
Email: [bscharf@vt.edu](mailto:bscharf@vt.edu)

## Present address

Lam Vo, Molecular Cellular and Developmental Biology and Physics, Yale University, New Haven, Connecticut, USA.

## Funding information

National Science Foundation, Grant/Award Number: IOS-1855066, MCB-1253234, MCB-1715185, MCB-1817652 and MCB-2128232

## Abstract

The bacterial flagellum is a complex macromolecular machine that drives bacteria through diverse fluid environments. Although many components of the flagellar motor are conserved across species, the roles of FliL are numerous and species-specific. Here, we have characterized an additional player required for flagellar motor function in *Sinorhizobium meliloti*, MotF, which we have identified as a FliL paralog. We performed a comparative analysis of MotF and FliL, identified interaction partners through bacterial two-hybrid and pull-down assays, and investigated their roles in motility and motor rotation. Both proteins form homooligomers, and interact with each other, and with the stator proteins MotA and MotB. The  $\Delta motF$  mutant exhibits normal flagellation but its swimming behavior and flagellar motor activity are severely impaired and erratic. In contrast, the  $\Delta fliL$  mutant is mostly aflagellate and nonmotile. Amino acid substitutions in cytoplasmic regions of MotA or disruption of the proton channel plug of MotB partially restored motor activity to the  $\Delta motF$  but not the  $\Delta fliL$  mutant. Altogether, our findings indicate that both, MotF and FliL, are essential for flagellar motor torque generation in *S. meliloti*. FliL may serve as a scaffold for stator integration into the motor, and MotF is required for proton channel modulation.

## KEYWORDS

chemotaxis, flagellar-basal body, proton channel plug, swimming motility, torque generation

## 1 | INTRODUCTION

Bacterial flagellar motility is a complex process whereby chemotactic signals culminate in the control of flagellar motor rotation to drive bacteria toward favorable and away from harmful conditions. The extensive evolutionary history and distinct selective pressures imparted by diverse environmental habitats correspond to the variability found in the regulation, structure, and function of the flagellar machinery from diverse bacterial species (Carroll & Liu, 2020; Imada, 2018; Rossmann & Beeby, 2018; Schuhmacher et al., 2015; Subramanian & Kearns, 2019; Wadhwa & Berg, 2021). Nonetheless, a core set of flagellar structural features are conserved

across the bacterial kingdom. The basal body at the proximal end of the flagellum is anchored in the cell membrane and is comprised of a trans-envelope axial rod and connected to the MS-ring in the inner membrane and the C-ring on the cytoplasmic face of the MS-ring (Kinoshita et al., 2018). A peptidoglycan-associated P-ring and lipopolysaccharide-associated L-ring together form a bushing between the rod and cell wall components during flagellar rotation (Kaplan et al., 2020). A short flexible hook is attached to the extracellular end of the rod and is followed by a rigid helical flagellar filament of up to several microns in length (Berg, 2003).

Rotation of the continuous basal body-hook-filament structure is mediated by conversion of ion motive force formed across the

This is an open access article under the terms of the [Creative Commons Attribution-NonCommercial-NoDerivs](https://creativecommons.org/licenses/by-nc-nd/4.0/) License, which permits use and distribution in any medium, provided the original work is properly cited, the use is non-commercial and no modifications or adaptations are made.

© 2022 The Authors. *Molecular Microbiology* published by John Wiley & Sons Ltd.

inner membrane into rotational energy by stator proteins MotA and MotB (or PomA and PomB in the Na<sup>+</sup>-driven motors of *Vibrio* species). Between 11 and 18 stator units form studs around the rotor, with each stud consisting of five MotA and two MotB units (Hu et al., 2021; Kaplan et al., 2019; Santiveri et al., 2020). Each MotA monomer contains four transmembranes (TM) helices with a large cytoplasmic loop between TM2 and TM3 and a cytoplasmic C-terminal tail distal to TM4 (Blair & Berg, 1990). MotB contains a short cytoplasmic N-terminal domain followed by a transmembrane domain, and a large periplasmic domain comprised of a proton channel plug region and an OmpA-like peptidoglycan-binding domain near the C-terminus (De Mot & Vanderleyden, 1994; Hosking et al., 2006; Kojima et al., 2018). Prior to assembling into the flagellar motor, inactive stator complexes form in the inner membrane with one MotB dimer surrounded by a MotA pentamer (Deme et al., 2020; Santiveri et al., 2020; Wadhwa & Berg, 2021). Two proton channels formed by the transmembrane domains of MotA and MotB are locked in a closed state by the periplasmic plug regions of each MotB monomer wedged between short periplasmic stretches of MotA. Once contact is made between the cytoplasmic loop of MotA and the C-ring component FliG, conformational changes in the stator units cause extension of the MotB periplasmic domains such that the peptidoglycan-binding domain of MotB associates with peptidoglycan to stabilize the stators near the basal body and the proton channel plug of MotB assumes an open conformation (Kojima et al., 2009, 2018; Morimoto et al., 2010; Roujeinikova, 2008; Van Way et al., 2000; Zhu et al., 2014). As protons flow through the now-open stator proton channels, conformational changes in the MotA<sub>5</sub>B<sub>2</sub> complexes cause clockwise rotation of the MotA pentamer around the MotB dimer, which—through interactions between MotA and FliG—imparts opposite rotation of the axial components of the flagellum to provide thrust (Wadhwa & Berg, 2021).

In the last two decades, another ubiquitous flagellar motor component, FliL, has gained considerable attention given its variable roles in flagellar motility (Figure S1). FliL is a membrane protein that is primarily localized in the periplasm where it is generally thought to interact with MotA and MotB. However, *fliL* mutant phenotypes differ considerably across the bacterial kingdom and a definitive role for FliL has yet to be determined. In several bacterial species, FliL has been implicated in various aspects of stator activity including stator assembly, association with the rotor, torque generation, surface sensing, and proton channel modulation as well as roles in flagellar filament (or rod) stability and orientation (Aldridge & Jenal, 1999; Attmannspacher et al., 2008; Belas et al., 2009; Belas & Suvanasthi, 2005; Chawla et al., 2017; Cusick et al., 2012; Fabela et al., 2013; Jenal et al., 1994; Kumar et al., 2017; Lee et al., 2013; Lin et al., 2018; Mengucci et al., 2020; Motaleb et al., 2011; Partridge et al., 2015; Pecina et al., 2021; Raha et al., 1994; Schoenhals & Macnab, 1999; Segura et al., 2001; Suaste-Olmos et al., 2010; Tachiyama et al., 2022; Takekawa et al., 2019; Zhu et al., 2015).

Efficient flagellar-driven movement in bacterial chemotaxis depends on the extension of run lengths in favorable directions and the increase of tumbling events to reorient bacteria when less favorable

conditions are detected. In peritrichous bacteria, runs are driven by synchronous rotation of several flagella in a propulsive flagellar bundle to provide thrust. Tumbling events are caused by disruption of the flagellar bundle when one or more flagella switch the direction of rotation from counterclockwise to clockwise or by slowing or pausing flagellar rotation (Subramanian & Kearns, 2019). Tumbling mechanisms are best understood in the switch-type motors of *Escherichia coli* and *Salmonella typhimurium*, whereby the phosphorylated response regulator CheY binds to the C-ring (switch) components FliM and FliN causing conformational changes that result in a greater C-ring diameter (Chang et al., 2020). This restructuring of the C-ring causes reorganization of MotA-FliG contacts such that continued clockwise rotation of the stator units now drives clockwise rotation of the rotor (Deme et al., 2020; Hu et al., 2021). The soil-dwelling plant symbiont *Sinorhizobium meliloti* employs a speed-variable unidirectional flagellar motor, which rotates solely in the CW direction and asynchrony of flagellar motor rotation induces bundle separation and cell tumbling (Attmannspacher et al., 2005). Molecular corollaries to these observations are found with the presence of additional motor proteins in *S. meliloti*, namely a periplasmic protein MotC and its chaperone MotE (Eggenhofer et al., 2004; Platzer et al., 1997). MotC is believed to interact with MotB; however, its role in flagellar motor function has yet to be elucidated.

Here, we describe MotF as a novel flagellar motor component and paralog of FliL in *S. meliloti*. MotF and FliL possess one transmembrane domain and reside mostly in the periplasm where both proteins engage in interactions with the stator components MotA and MotB. However, while  $\Delta motF$  and  $\Delta fliL$  mutants exhibit severe reductions in swimming motility and defects in flagellar motor function, a very small population of the normally flagellated  $\Delta motF$  mutant retains poor swimming motility while the generally aflagellate  $\Delta fliL$  mutant is nonmotile. Furthermore, we demonstrate that second-site mutations in the stator components MotA or MotB partially restore motility to the  $\Delta motF$  but not the  $\Delta fliL$  mutant.

## 2 | RESULTS

### 2.1 | Identification of three new flagellar genes and one new motor gene in *Sinorhizobium meliloti*

In a search of additional genes involved in *S. meliloti* motility, a mini-Tn5 transposon mutagenesis screen of the wild-type *S. meliloti* strain RU11/001 was carried out on soft agar swim plates. Upon sequencing of transposon insertion sites for 26 mutants with observed motility defects, the majority of insertions occurred within known flagellar genes. One mutant, however, contained an insertion in the gene locus *SMc03057*, which is one of four uncharacterized genes clustered immediately downstream of *fliR*, the last annotated gene of the contiguous flagellar regulon on the *S. meliloti* chromosome (Figure 1a). To confirm that *SMc03057* contributes to flagellar motility and to determine the role of the other three genes in motility, strains with in-frame deletions were constructed and tested

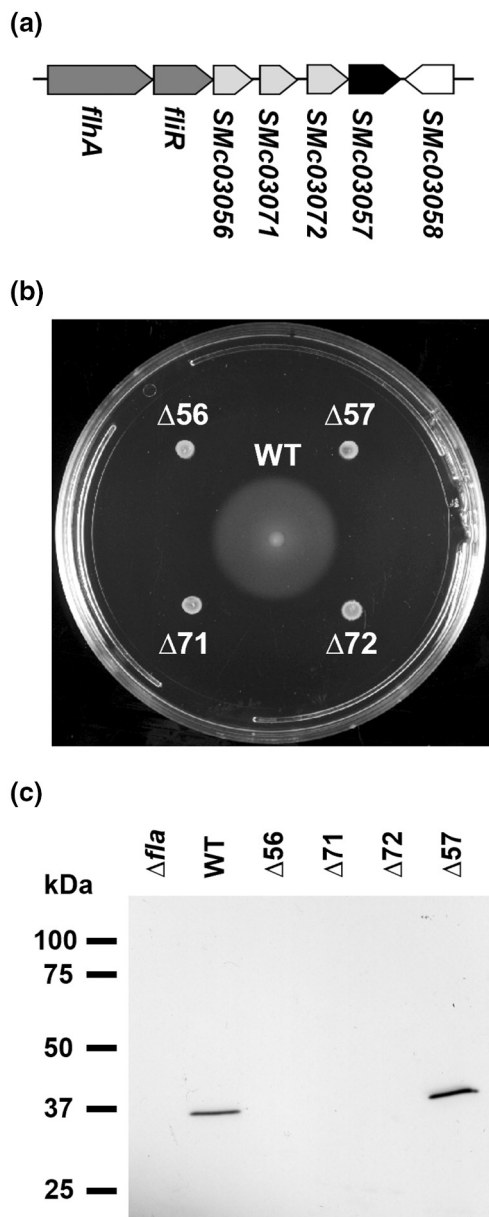


**FIGURE 1** Identification of genes required for flagellar motility in *S. meliloti*. (a) Genomic context of four uncharacterized motility genes located on the *S. meliloti* chromosome downstream of *flhR*, the last gene in the flagellar regulon. The currently annotated flagellar genes *flhA* and *flhR* are shown in dark gray, structural genes *SMc03056*, *SMc03071*, and *SMc03072* are shown in light gray, *SMc03057* (renamed *motF* in this study) is shown in black, and a putative glycosyltransferase gene, *SMc03058*, encoded on the (-) strand, is shown in white. (b) Swim ring analysis of in-frame deletions of *SMc03056* ( $\Delta 56$ ), *SMc03071* ( $\Delta 71$ ), *SMc03072* ( $\Delta 72$ ), and *SMc03057* ( $\Delta 57$ ) compared to wild type (WT). Stationary phase cultures (3  $\mu$ l) of each strain were transferred onto swim plates and incubated at 30°C for 3 days. (c) Anti-flagellin immunoblot analysis of wild type,  $\Delta 56$ ,  $\Delta 71$ ,  $\Delta 72$ , and  $\Delta 57$ . A mutant lacking all four flagellin genes ( $\Delta fla$ ) was used as a negative control.

for swimming proficiency on soft agar swim plates (Figure 1b). All four mutants exhibited a loss of motility in this assay. A BLAST search of the gene products revealed that *SMc03071* shares

**TABLE 1** Predicted molecular weight and function of newly discovered motility genes

Protein	Molecular weight (kDa)	Description
SMc03056	15.3	Hypothetical protein
SMc03071	19.5	Flg <sub>N</sub> rod-binding protein
SMc03072	13.5	FlgN flagella synthesis protein
SMc03057 <sup>a</sup>	20.5	FliL-like protein

<sup>a</sup>Renamed *MotF*.

homology with the N-terminal rod-binding domain of FlgJ (Flg<sub>JN</sub>) while *SMc03072* is a homolog of the type-three secretion system chaperone FlgN involved in the secretion of the hook-associated proteins FlgK and FlgL (Aldridge et al., 2003; Hirano et al., 2001). A search with *SMc03057* resulted in matches with a FliL-like protein in *Agrobacterium tumefaciens* or hypothetical proteins in an array of alphaproteobacteria, while *SMc03056* did not yield any homology or domain similarities to other characterized proteins using SignalP, TMHMM, and Pfam (Table 1) (Krogh et al., 2001; Mistry et al., 2021; Teufel et al., 2022).

Flagellar gene transcription and biosynthesis occur in a hierarchical manner with the production of flagellin and assembly of the filament taking place after completion of the basal body and hook structures (Berg, 2003; Rotter et al., 2006). Therefore, to determine if any of these genes are required for flagellar synthesis, we analyzed the production of flagellin proteins by immunoblot analysis. Three of the four mutants did not produce flagellin; however, the  $\Delta SMc03057$  strain produced flagellin at levels comparable to wild type (Figure 1c). In agreement with these results, we found that the promoter activity of the principle flagellin gene *flaA* (*PflaA*) was markedly reduced for the three mutants lacking flagellin production throughout the motility phase of cell culture growth when compared to the wild type (Figure S2). Such downregulation of *flaA* transcription has been reported for mutants defective in basal body production (Sourjik et al., 2000). This result was expected for  $\Delta SMc03071$  and  $\Delta SMc03072$  considering the predicted structural roles of Flg<sub>JN</sub> and FlgN in basal body synthesis. These analyses also categorized the hypothetical gene *SMc03056* as a flagellar assembly or structural gene. In contrast, the *flaA* promoter activity in the  $\Delta SMc03057$  strain was mostly comparable to wild type (Figure S2). The finding that the deletion of *SMc03057* resulted in a non-motile (Figure 1b) but flagellin-producing mutant (Figures 1c and S2) defined it as a motility gene, and we thus named it *motF*. The  $\Delta motF$  motility defect was complemented upon ectopic expression from a self-replicating plasmid (Figure S3). When the  $\Delta motF$  strain was viewed by phase-contrast microscopy, most of the cells in the population were nonmotile. Interestingly, a very small percentage of cells exhibited slow swimming motility interrupted by frequent jerking and pauses and abrupt directional changes. Altogether, these results suggested that *MotF* is required for flagellar function but not synthesis and its role in motility was further characterized.

## 2.2 | MotF is a distantly related paralog of *S. meliloti* FliL

An NCBI BLASTP search of the nonredundant database with the MotF amino acid sequence yielded results for many hypothetical proteins from various rhizobial species as well as proteins from the FliL family in *Agrobacterium tumefaciens* (51% identity) and *Rhizobiaceae* bacterium LC148 (49% identity). FliL is described as an enigmatic protein with diverse roles in flagellar swimming and swarming in *E. coli*, *S. typhimurium*, *Vibrio alginolyticus*, *Rhodobacter sphaeroides*, *Caulobacter crescentus*, and *Bradyrhizobium diazoefficiens*, surface sensing in *Proteus mirabilis*, and flagellar orientation in *Borrelia burgdorferi* (Figure S1) (Attmannspacher et al., 2008; Fabela et al., 2013; Jenal et al., 1994; Kumar et al., 2017; Lee & Belas, 2015; Lin et al., 2018; Mengucci et al., 2020; Motaleb et al., 2011; Partridge et al., 2015; Raha et al., 1994; Schoenhals & Macnab, 1999; Suaste-Olmos et al., 2010; Zhu et al., 2015). The flagellar regulon of *S. meliloti* contains a gene annotated as *fliL* located between the L-ring encoding *flgH* and the flagellar biosynthetic gene *fliP* (Figure S4). However, the role of FliL in *S. meliloti* swimming motility had yet to be determined. Multiple sequence alignment and phylogenetic tree analysis of *S. meliloti* MotF and FliL with FliL sequences from diverse bacterial species revealed that *S. meliloti* FliL aligns more closely with FliL from other species than with *S. meliloti* MotF (Figure S5 and Table S1) implying that MotF is a FliL paralog with substantial evolutionary divergence from the ancestral protein. It should be noted that the genomes of *V. alginolyticus* and *R. sphaeroides* encode two *fliL* gene copies. However, each FliL functions separately in independent flagellar motor systems in these two species (Mengucci et al., 2020; Takekawa et al., 2019).

Next, we used AlphaFold Colab to generate a MotF structure prediction (Figure 2a) (Jumper et al., 2021). The predicted structure contains an N-terminal alpha-helix (aa 1–25) followed by a short, disordered region (aa 26–32) and a short alpha-helix (aa 33–41). A globular domain (aa 42–144) comprised of four alpha-helices and three beta-sheets is followed by a mostly disordered C-terminal region (aa 145–187). We then submitted the putative MotF structure to the DALI server to identify proteins with similar folds. The top hit was the *V. alginolyticus* FliL<sub>40-167</sub> structure (Figure 2b) (Takekawa et al., 2019). An alignment of both structures reveals that the globular MotF domain shares a high similarity to the core of *V. alginolyticus* FliL despite low sequence conservation (Figure 2c,d). Altogether, these data indicate that MotF is a highly divergent FliL paralog in *S. meliloti* and related bacteria.

## 2.3 | The *fliL* deletion mutant is nonmotile and exhibits reduced flagellation and *flaA* gene transcription

The evolutionary relatedness of MotF and FliL led us to an initial motility assessment of an in-frame *fliL* deletion mutant. The  $\Delta fliL$  strain is nonmotile on soft agar swim plates (Figure 3a) and appeared

similarly nonmotile when observed by phase-contrast microscopy. Unsurprisingly, the  $\Delta fliL \Delta motF$  double mutant was also nonmotile on swim plates (data not shown). We used immunoblot analysis to compare flagellin levels in the  $\Delta fliL$  strain with wild type, the  $\Delta motF$  strain, and a  $\Delta flaA$  strain, which has previously been shown to exhibit reduced flagellation (Figure 3b) (Scharf et al., 2001). The  $\Delta fliL$  strain exhibited substantially reduced flagellin levels comparable to the  $\Delta flaA$  strain. Additionally, while the wild type and the  $\Delta motF$  strain were similarly flagellated as determined by transmission electron microscopy, the  $\Delta fliL$  strain was mostly aflagellate (Figure 3c). Complementation of the  $\Delta fliL$  mutant by ectopic expression of *fliL* confirmed that the swimming defect is not caused by the polar effects of the mutation (Figure 3a). It has previously been reported that the *S. enterica*  $\Delta fliL$  strain exhibits a flagellar rod-breakage phenotype that is overcome by paralyzing the flagellar motor (Attmannspacher et al., 2008). To test whether this is the case for *S. meliloti*  $\Delta fliL$ , we additionally deleted *fliL* in the  $\Delta motA$  strain. Flagellin production in the  $\Delta motA \Delta fliL$  double mutant was reduced to levels comparable to the  $\Delta fliL$  strain indicating that the reduced flagellin levels of the single mutant are not caused by loss of rod stabilization by FliL (Figure 3c).

To determine whether the loss of FliL causes dysregulation of *flaA* transcription, we investigated PflaA activity in the  $\Delta fliL$  strain (Figure 3d). Transcription of *flaA* was about 50% reduced compared to wild type or the *motF* deletion strain, which both exhibit normal flagellation. Furthermore, the reduction of PflaA was greater than that of the  $\Delta fliM$  strain, which served as a measure for low PflaA activity due to feedback inhibition by the accumulation of intracellular flagellin (Sourjik et al., 2000). In conclusion, the presence of FliL is required for wild-type PflaA gene transcription and production of flagellar filaments, whereas MotF appears more strictly linked to flagellar motor function.

## 2.4 | MotF protein architecture resembles that of FliL

All known FliL proteins have a short (comprised of less than 15 aa) N-terminal region in the cytoplasm and a single transmembrane domain, with the remainder of the protein residing in the periplasm. Bioinformatics analysis of *S. meliloti* FliL using the TMHMM server for transmembrane domain prediction was in good agreement with this protein organization: aa 1–12 were predicted to be localized in the cytoplasm, aa 13–35 to form a transmembrane helix, and aa 36–163 to be localized in the periplasm (Figure 2a) (Partridge et al., 2015; Takekawa et al., 2019). A domain prediction for *S. meliloti* MotF by TMHMM yielded similar results (Krogh et al., 2001). In contrast, consensus predictions by programs such as SignalP 5.0 suggested that the hydrophobic N-terminal region in MotF serves as a signal peptide with a canonical AXA signal peptidase I cleavage site after aa 28 for secretion of the protein into the periplasm (Figures 2a and 4a). If MotF (20.5 kDa) is translated as a pre-protein, the cleavage by a signal peptidase would yield a mature MotF (MotF\*) of

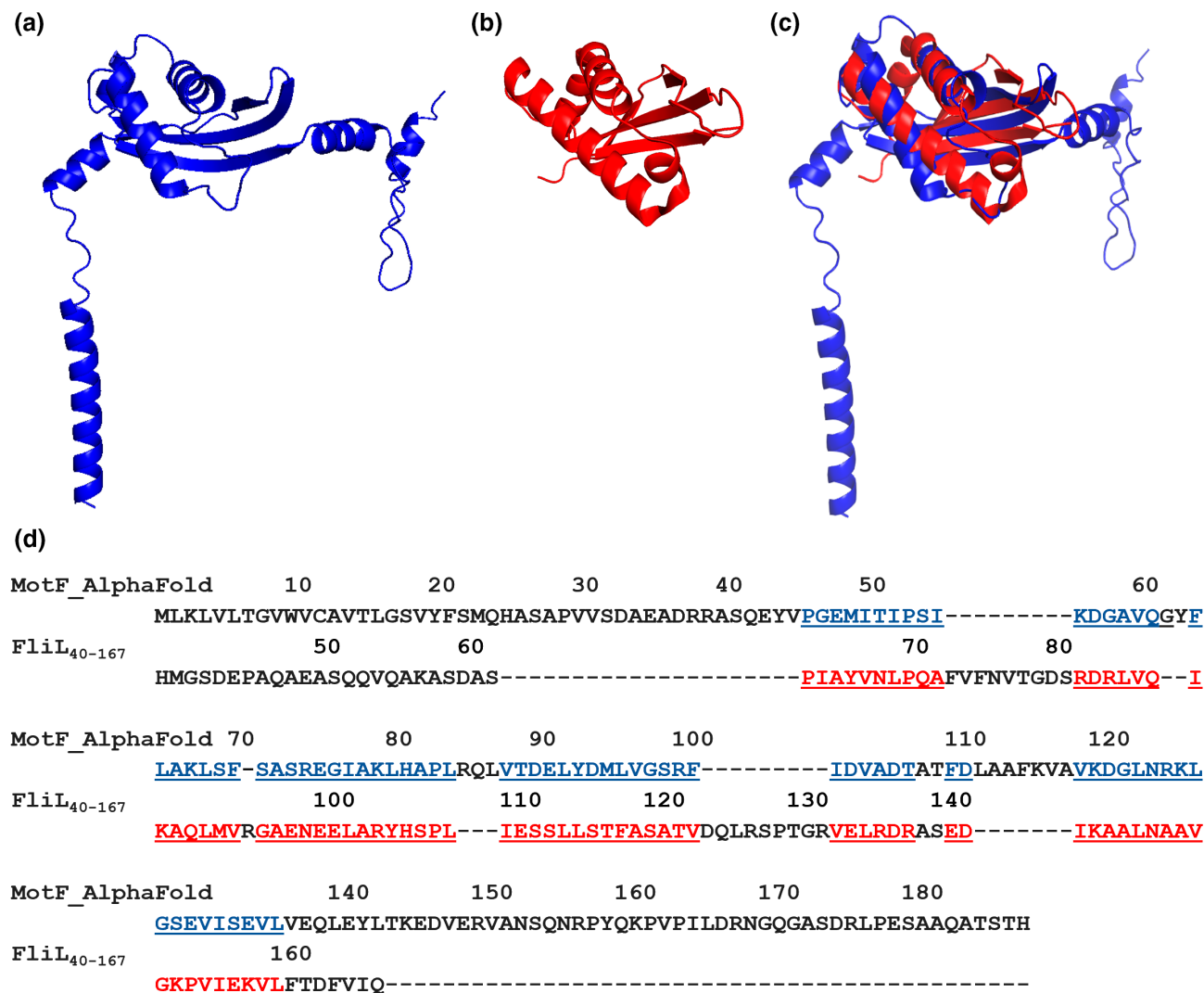


FIGURE 2 Structural modeling of MotF. (a) AlphaFold structural model of *S. meliloti* MotF. (b) Ribbon diagram of *V. alginolyticus* FliL<sub>40-167</sub> (PDB ID: 6AHQ). (c) *S. meliloti* MotF (blue) aligned to *V. alginolyticus* FliL<sub>40-167</sub> (red). (d) Structure-based amino acid sequence alignment of *S. meliloti* MotF and FliL<sub>40-167</sub>.

17.5 kDa. To investigate the size of MotF and to gain insight into its subcellular location, a series of biochemical analyses were performed. Immunoblot analysis of *S. meliloti* wild-type cell lysates detected MotF at the full-length size of 20.5 kDa compared to purified recombinant MotF\* at 17.5 kDa indicating that MotF is not being cleaved (Figure 4a). To confirm that MotF is localized to the membrane via its N-terminal transmembrane domain, we performed cell fractionation experiments and probed for MotF in the soluble and membrane fractions (Figure 4b). The majority of MotF was detected in the membrane fraction. The small amount of MotF in the cytoplasm likely stems from translated protein that has yet to be inserted into the membrane.

Next, we sought to determine the orientation of the MotF transmembrane domain by employing the dual reporter plasmid system pKTop (Karimova et al., 2009; Karimova & Ladant, 2017). The pKTop system drives the production of a fusion protein comprised of a protein of interest translationally fused at the

C-terminus to the *E. coli* alkaline phosphatase (AP, encoded by *phoA*) and the alpha subunit of  $\beta$ -galactosidase (encoded by *lacZ* $\alpha$ ), which are only active in the periplasm and cytoplasm, respectively. Periplasmic AP converts the substrate X-Pho to an insoluble blue precipitate while cytoplasmic LacZ $\alpha$  converts a substrate Red-Gal to an insoluble red precipitate. Control plasmids include the unmodified pKTop plasmid, which produces a AP-LacZ $\alpha$  fusion protein that remains in the cytoplasm, and a periplasmic control plasmid encoding the first outward-facing transmembrane domain of *E. coli* YmgF (YmgF<sub>1-39</sub>) fused to AP-LacZ $\alpha$  (Karimova et al., 2009; Karimova & Ladant, 2017). When we introduced a pKTop derivative harboring the full-length *motF* coding sequence into *E. coli* DH5 $\alpha$  and plated transformants on LB agar supplemented with X-Pho, we observed blue coloration comparable to a periplasmic control strain indicating that the C-terminus of MotF is located in the periplasm (Figure 4c). To confirm that the MotF transmembrane domain alone is sufficient to place PhoA-LacZ $\alpha$  in



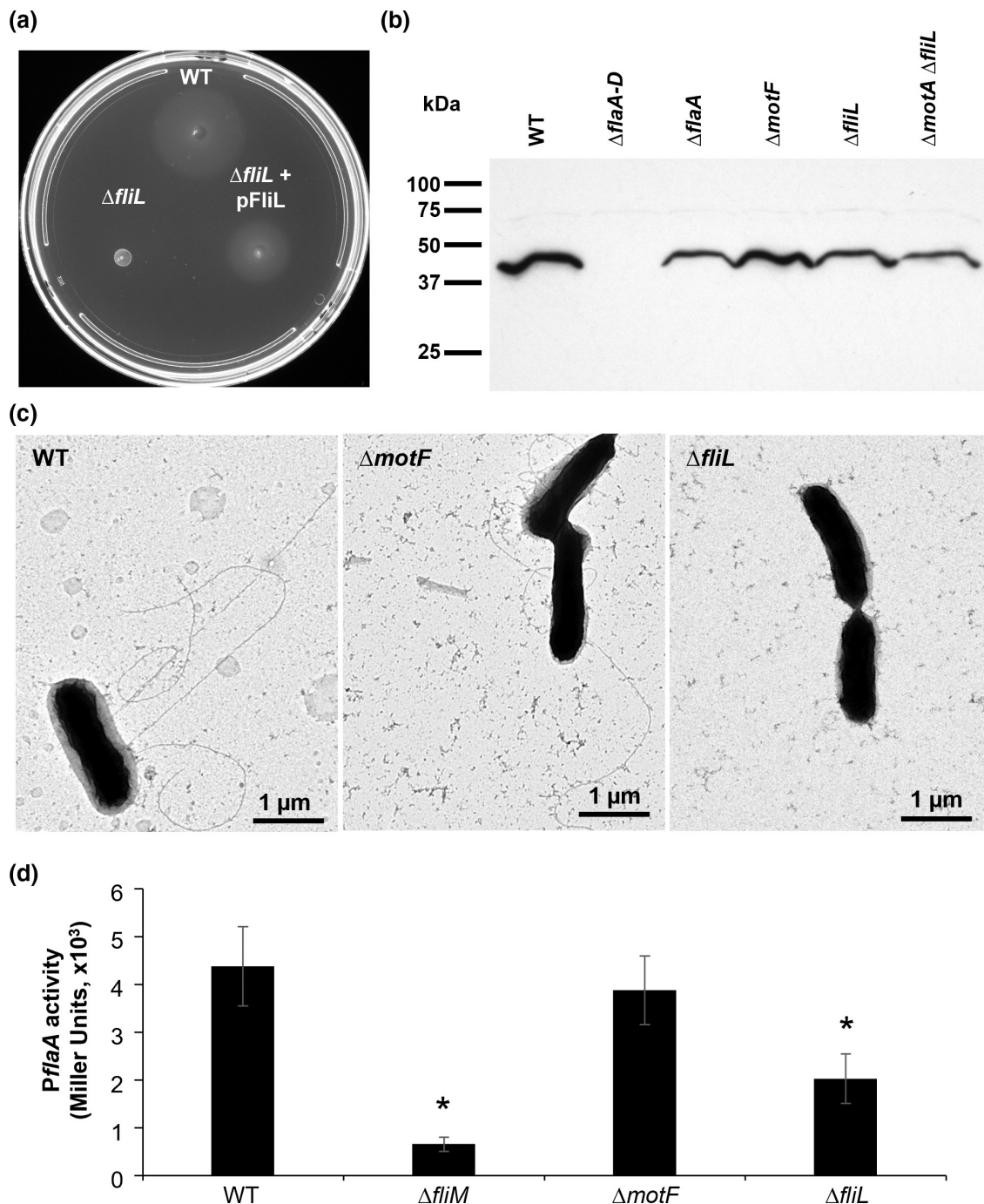


**FIGURE 3** Motility behavior and flagellation of the  $\Delta fliL$  strain. (a) Swim ring analysis of wild type,  $\Delta fliL$  and  $\Delta fliL$  complemented *in trans*. (b) Anti-flagellin immunoblot analysis of wild type,  $\Delta flaA-D$ ,  $\Delta flaA$ ,  $\Delta motF$ ,  $\Delta fliL$ , and  $\Delta motA \Delta fliL$  cell cultures. (c) Transmission electron microscopy (TEM) analysis of wild type (WT),  $\Delta motF$ , and  $\Delta fliL$  grown in Bromfield overlay cultures. Bacteria were fixed in 2% glutaraldehyde and stained with 1% uranyl acetate. (d) The activity of the *flaA* promoter in wild type,  $\Delta motF$ ,  $\Delta fliL$ , and  $\Delta fliM$  as negative control. Shown are the averages and standard deviations of  $\beta$ -galactosidase activity for three independent experiments with three technical replicates each. Asterisks (\*) indicate a significant difference from the wild type ( $p < .02$ ).

the periplasm, we introduced the corresponding MotF coding region (aa 1–28) into pKTop. Transformants harboring this construct also produced a blue coloration. Altogether, these data demonstrate that MotF contains an N-terminal transmembrane domain and that the majority of the protein is located in the periplasm similar to FliL homologs characterized to date.

## 2.5 | The MotF interactome resembles the FliL interactome

FliL from *S. enterica* and *V. alginolyticus* have been reported to exhibit self-interaction, as well as interactions with the MS ring component FliF and the stator proteins MotA and MotB (Partridge et al., 2015; Takekawa

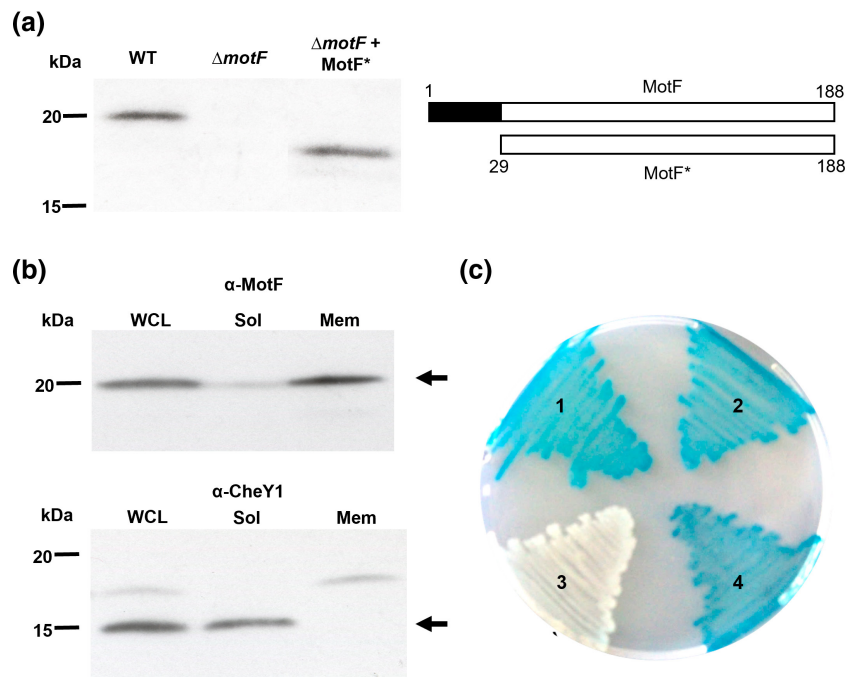


**FIGURE 4** Subcellular localization and topology of MotF. (a) Anti-MotF immunoblot analysis of wild type (WT) cell lysates compared to purified MotF lacking the predicted signal sequence (MotF\*) in  $\Delta motF$  cell lysates. The topologies of the detected proteins are illustrated to the right. (b) Immunoblot analysis of MotF (top panel) and CheY1 (bottom panel) in subcellular fractions. The MotF and CheY1 bands are indicated by arrows. Lys, whole-cell lysate; sol, soluble fraction; mem, membrane fraction. (c) MotF topology analysis in an alkaline phosphatase (AP) reporter assay. *E. coli* DH5 $\alpha$  with pKTop expressing AP fusion proteins with full-length MotF (1), the MotF transmembrane domain (2), unmodified AP (3), or the periplasmic control YmgF<sub>1-39</sub> (4) were incubated on LB agar plates supplemented with the chromogenic substrate X-pho. The blue color indicates the periplasmic localization of the C-terminus of the expressed protein.

et al., 2019). To determine how *S. meliloti* FliL and MotF compare in their respective interactomes to FliLs from other species, we performed bacterial two-hybrid (BACTH) analyses for FliL and MotF with various basal body and stator components using MacConkey plates and quantitative colorimetric  $\beta$ -galactosidase assays. We transformed *E. coli* BTH101  $\Delta flhC$  with pKT25 and pUT18C derivatives to avoid interference from the host flagellar machinery (Partridge et al., 2015). Similar to previous reports with other FliLs, we determined that *S. meliloti* FliL interacts strongly with itself and moderately with both stator components MotA and MotB (Figure 5a,b). The BACTH data suggested that FliL interacts with FliF but not FliG while the  $\beta$ -galactosidase data showed the opposite. However, it should be noted that Partridge et al. also reported weak and inconsistent interactions between FliL and both basal body components (Partridge et al., 2015). Intriguingly, FliL interacted strongly with MotF. When we performed the BACTH experiments with MotF and the various basal body and stator components, we found similar interaction as described above for FliL. MotF interacted strongly with itself and FliL, moderately with MotA, and weakly with MotB and possibly FliF, but not with FliG (Figure 5c,d). Control experiments with protein pairs such as MotA/MotA and MotA/MotB yielded the expected positive interactions (Table S2). However, interactions could not be detected between other known interacting pairs such as MotA/FliG and FliF/FliG, perhaps due to limitations of expressing functional and/or stable FliF and FliG proteins in the heterologous *E. coli* host. Altogether, these results demonstrate that *S. meliloti* FliL and its paralog MotF form homooligomers, interact with each other, and interact with both stator components.

To provide additional evidence of MotF interaction partners, we performed immobilized metal affinity chromatography (IMAC) pull-down assays. Candidate interaction partners, each fused N-terminally to a 6xHis tag, were used as bait, coexpressed with MotF as prey, pulled down via IMAC, and assayed using anti-MotF antiserum. We also included MotC in this experiment, which is an alphaproteobacteria-specific protein that is required for flagellar motor function in *S. meliloti* (Platzer et al., 1997). The cytoplasmic chemotaxis protein CheR was employed as a negative control. As seen in Figure 6, MotF could be detected robustly in pull-down fractions with 6xHis-FliL and 6xHis-MotA, weakly with 6xHis-MotC, and very weakly with 6xHis-MotB, but not with, -FliF, -FliG, or -CheR. Importantly, we were able to detect all our bait proteins with an anti-His-antibody in corresponding soluble and pull-down fractions except for FliF, presumably due to solubilization issues (data not shown). Altogether, these data further indicate that MotF and FliL interact with each other and that MotF interacts with MotA, MotB, and MotC.

## 2.6 | The periplasmic domain of MotF forms multimers and interacts with MotC and the periplasmic domain of MotB

We next tested whether the periplasmic region of MotF (MotF\*) alone can interact with the periplasmic regions of MotB (MotB\*) and FliL (FliL\*), and with MotC by BACTH analysis and in vitro cross-linking with purified proteins. The BACTH assay detected

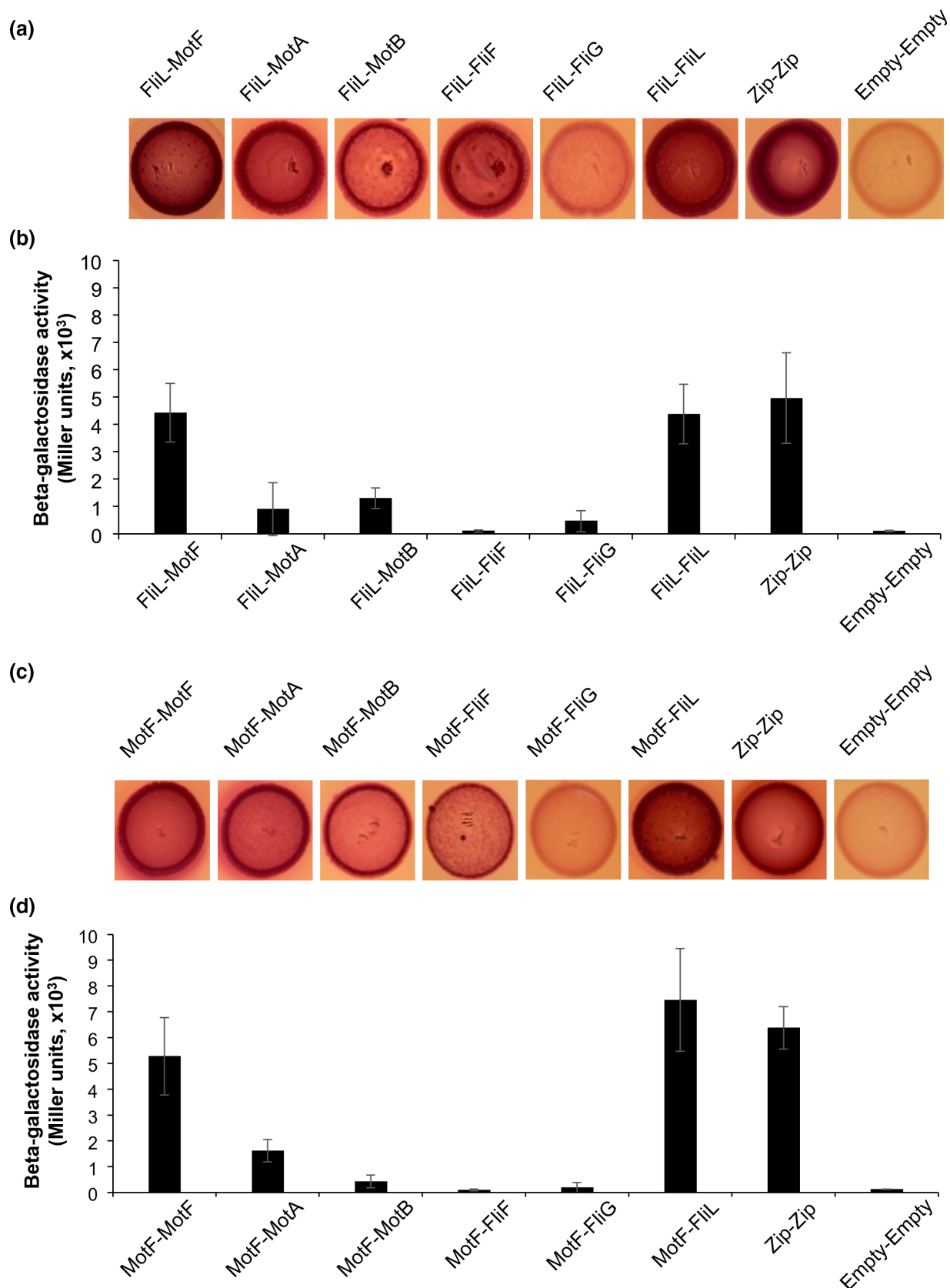


**FIGURE 5** Bacterial two-hybrid (BACTH) assays of FliL and MotF interactions with basal body components. FliL and the indicated proteins were tested for interaction in *E. coli* BTH101  $\Delta fliH$  cells on MacConkey/lactose plates at 30°C for 48 h (a) and by  $\beta$ -galactosidase assays (b); MotF and the indicated proteins were tested for interaction in *E. coli* BTH101  $\Delta fliH$  cells on MacConkey/lactose plates at 30°C for 48 h (c) and by  $\beta$ -galactosidase assays (d). Interaction pair labels correspond to proteins produced from pKT25 and pUT18C, respectively.



self-interactions for MotF\*, MotB\*, and FliL\* but not between different proteins (Table S3). It is conceivable to speculate that the conditions in the cytosolic environment were unresponsive of these

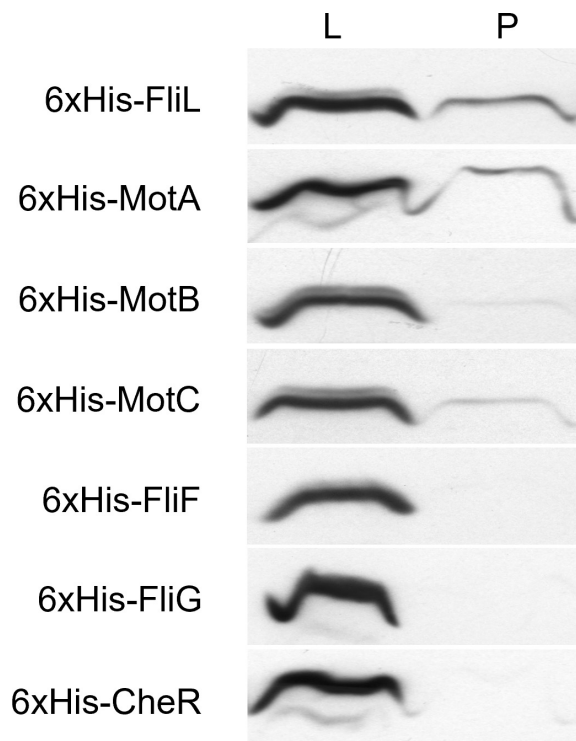


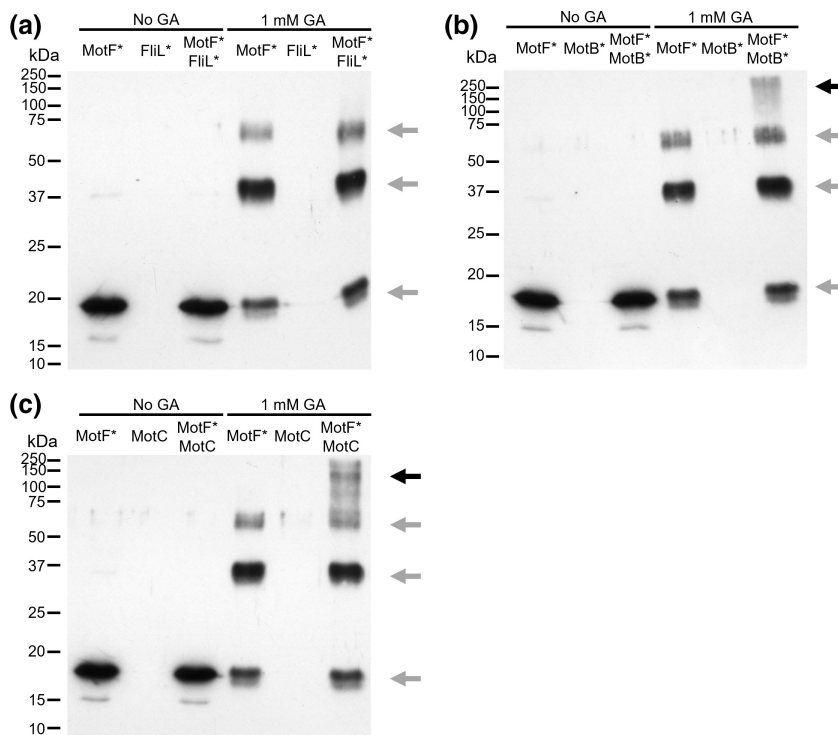
**FIGURE 6** Pull-down assays of MotF. Genes encoding putative MotF interaction partners were cloned in MCS-1 of pETDuet-1 to yield proteins N-terminally fused with a 6x-his tag; *motF* was cloned in MCS-2. Pull-down assays using IMAC were performed as described in the materials and methods. L, loaded fraction; P, pulled-down fraction.

protein–protein interactions. However, using in vitro cross-linking of purified proteins with glutaraldehyde, we detected interactions of MotF\* with MotB\* (Figure 7b) and with MotC (Figure 7c) but not with FliL\* (Figure 7a). MotF\* was detected as a monomer at ~18 kDa without crosslinker or as a monomer, homodimer (~36 kDa), and homotrimer (~54 kDa) when glutaraldehyde was present in the reaction mixture. In addition to these signals, we discovered high molecular weight complexes of 75–250 kDa in cross-linking reactions with MotF\* and MotB\* or MotC suggesting that they associate with and promote higher-degree MotF\* oligomerization. Taken together, we infer that the periplasmic domain of MotF is sufficient for the formation of homo-oligomers and to interact with MotB and MotC, but that MotF and FliL might associate via their transmembrane domains.

## 2.7 | MotF and FliL stabilize each other

We have shown that MotF and FliL interact with each other as well as with the stator components MotA and MotB. Thus, we asked whether interacting proteins promote the stability of interaction partners (Dixit & Maslov, 2013). To investigate this possibility, we first compared cellular levels of MotF in mutants lacking individual *mot* genes or *fliL*. As presented in Figure 8a, MotF levels in the  $\Delta motA$ ,  $\Delta motB$ , and  $\Delta motC$  strains are comparable to those in wild type and in the control strain  $\Delta cheY1$  implying that individual Mot proteins are not required for MotF stability. In contrast, MotF levels were reduced in the  $\Delta fliL$  strain suggesting that MotF requires FliL for stability (Figure 8a). We also investigated whether MotB, MotC, or FliL require MotF for normal cellular abundance (Figure 8b–d). While MotB and MotC levels in the  $\Delta motF$  strain were comparable to wild type, FliL levels were strongly reduced in the absence of MotF.

**FIGURE 7** In vitro glutaraldehyde cross-linking assay of the purified periplasmic domain of MotF (MotF\*) with (a) the periplasmic domain of MotB (MotB\*), (b) MotC, and (c) the periplasmic domain of FliL (FliL\*). Gray arrows mark different oligomeric states of MotF\* and black arrows mark the heterooligomers with MotF\* and MotB\* or MotC. Purified proteins at 1  $\mu$ M were incubated in the presence or absence of 1 mM glutaraldehyde for 1 h at room temperature prior to gel electrophoresis and immunoblot analysis with the anti-MotF antibody.



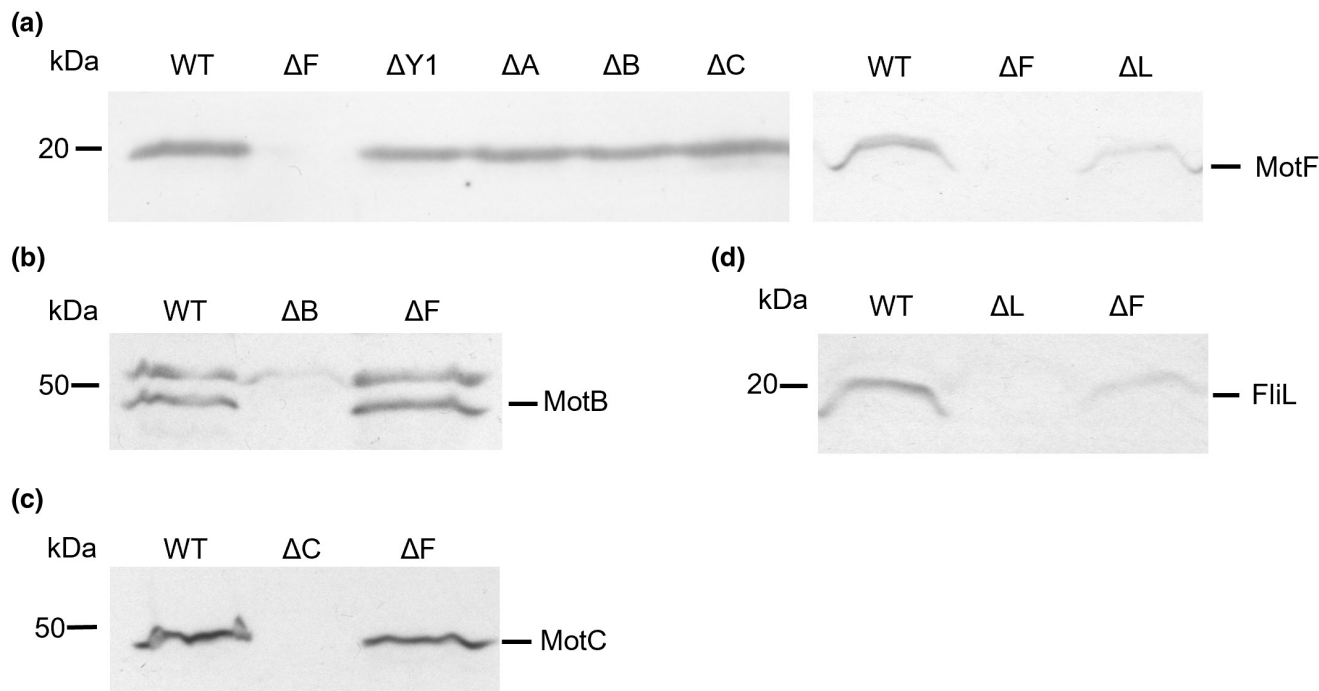


**FIGURE 8** Immunoblot analysis of cellular protein levels in wild type and deletion strains. Levels of MotF in various deletion strains (a). Levels of MotB (b), MotC (c), and FliL (d) in  $\Delta motF$ . Equal amounts of lysates from cells grown in Bromfield overlay cultures were analyzed using polyclonal antibodies raised against the specified protein.

Altogether, these results imply that the interaction between MotF and FliL promotes their stability and integration into the *S. meliloti* flagellar motor.

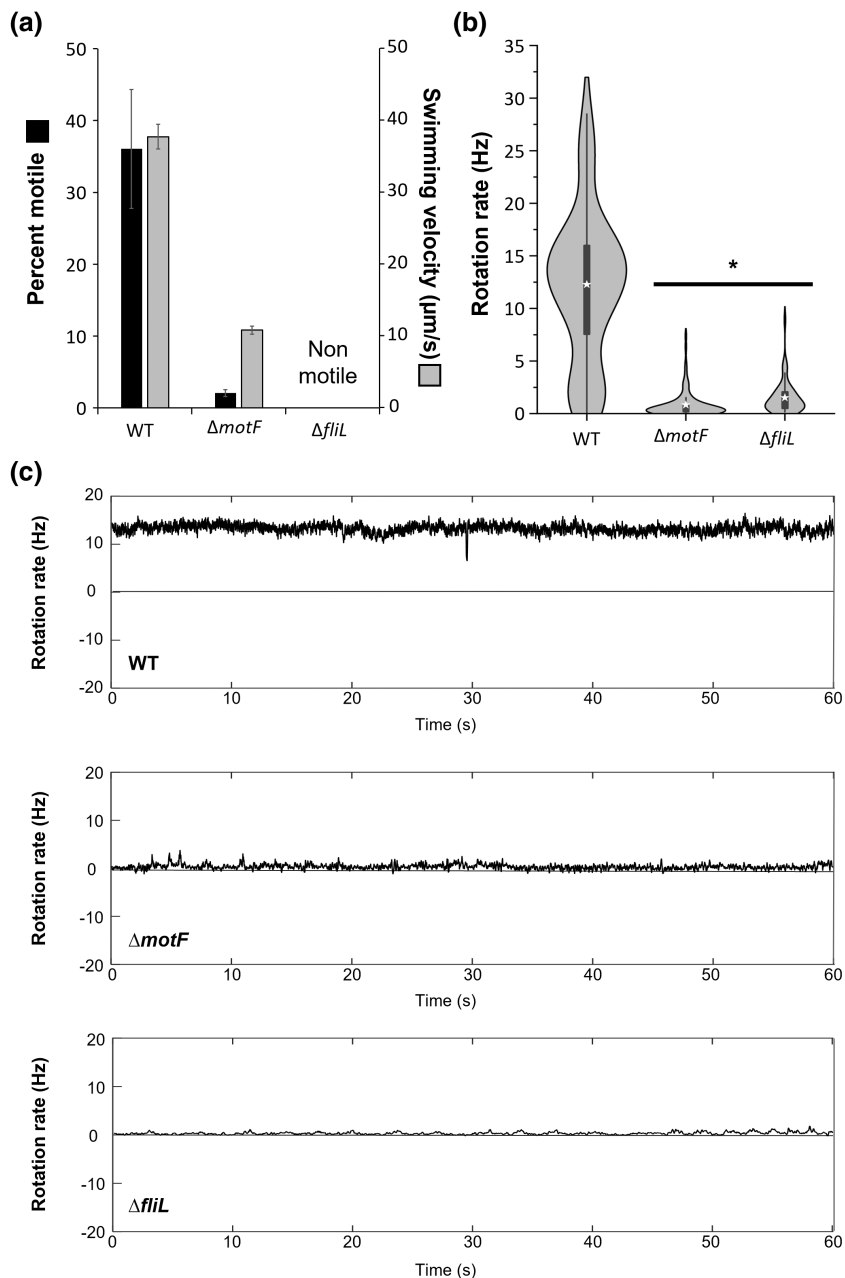
## 2.8 | The *motF* and *fliL* deletion strains exhibit severely impaired but distinct motility phenotypes

An initial test of the *motF* and *fliL* deletion strains showed that neither mutant is able to spread on soft agar plates (Figures 1b, 3a, and Figure S3). However, a quantitative analysis indicated that  $\Delta motF$  produces swim rings that are slightly larger than those formed by  $\Delta fliL$  (Figure S6). To thoroughly assess swimming motility behavior, we determined percentages of motile cells and free-swimming velocities of bacteria by phase-contrast microscopy and computerized motion analysis using TumbleScore (Pottash et al., 2017). The percentage of free-swimming  $\Delta motF$  cells was reduced by nearly 20-fold to  $2.1 \pm 0.5\%$  compared to  $36.0 \pm 8.2\%$  for the wild-type population (Figure 9a and Table 2). For the small motile population of  $\Delta motF$  cells, average swimming velocities were  $10.9 \pm 0.6 \mu\text{m/s}$ , which was about 70% lower than that of the wild type ( $37.7 \pm 1.7 \mu\text{m/s}$ ). Thus, the swimming defect exhibited by the  $\Delta motF$  strain is due to a substantial reduction of the motile population and severely reduced swimming velocity. The  $\Delta fliL$  strain was nonmotile, with the exception of an extremely low number of cells (<1%) that exhibited stationary rotational movement.

The decreased swimming capacity exhibited by  $\Delta motF$  could be caused by reduced flagellar motor rotation or the inability to

form a propulsive bundle due to a asynchronized rotation of flagellar motors along the cell. If the swimming defects are caused by a asynchronized rotation of the motors, we would expect to observe similar motor rotation rates for this mutant compared to the wild type. In contrast, if motors are generally defective in their rotation, then we would expect an overall decreased prevalence of rotating motors as well as diminished rotation rates. To distinguish between these possibilities, we performed cell tethering assays and analyzed motor behavior (Figure 9). Rotation rates of wild-type motors averaged approximately 12.5 Hz, as previously documented (Sourjik & Schmitt, 1996), with maximal rotation rates of up to 28 Hz (Figure 9b). In contrast, motor rotation rates of  $\Delta motF$  averaged at 0.8 Hz and reached a maximum rotation rate of 7.5 Hz, clearly indicating an overall diminished functional capacity. Further exemplifying this point, a representative graph depicting the activity of an individual wild-type motor over a 60-s time period revealed high overall rotation rates with brief fluctuations above and below the average of about 12 Hz (representative image shown in Figure 9c). The  $\Delta motF$  mutant consistently exhibited low-level rotation rates around 1 Hz with brief pulses of rotation above the average rotation rate interspersed between periods of no or low activity (Figure 9c). Additionally, the number of rotating  $\Delta motF$  bacterial cells was substantially reduced compared to wild type. These data demonstrate that the swimming defect exhibited by the *motF* deletion strain is caused by an inability to induce consistent motor rotation. Since a very small population of  $\Delta fliL$  cells exhibited stationary motion, we also quantified the motor rotation of this mutant in the tethered cell assay. The percentage of

**FIGURE 9** Swimming and flagellar motor behavior of *S. meliloti* wild type,  $\Delta motF$  and  $\Delta fliL$  in the tethered-cell assay. (a) Swimming velocity and percentage of motile bacteria. (b) Average rotation rates of single flagellar motors ( $n = 100$  for wild type and  $\Delta motF$ , and  $n = 40$  for  $\Delta fliL$ ). Asterisks mark average rotation rates and boxes correspond to the interquartile ranges. (c) Traces of representative rotation rates for each strain.



rotating  $\Delta fliL$  bacteria was far smaller than for the already severely defective  $\Delta motF$  strain but with similar average and maximum rotation rates (Figure 9b). In conclusion, the absence of MotF, and to an even greater degree of FliL, severely reduces the number of flagellar motors engaged in rotation. However, once motors are engaged, both deletion strains exhibit comparably abysmal rotation rates.

## 2.9 | Mutations in the stator genes *motA* and *motB* restore motility to the *motF* but not the *fliL* deletion strain

To further investigate the mechanism by which MotF and FliL contribute to flagellar motility, we imposed selective pressure to

produce second-site suppressor mutations in both deletion mutant backgrounds by extended incubation on soft agar swim plates. Under the conditions of this assay, motile bacteria exhibit a fitness advantage by swimming outward from the inoculum toward regions with higher levels of nutrients. Despite several attempts, we were unable to obtain  $\Delta fliL$  suppressor mutants. However, we independently isolated five  $\Delta motF$  suppressor mutants and found via whole-genome sequencing that all five strains contained single mutations in coding regions of *motA* corresponding to amino acid substitution G136S in the cytoplasmic loop connecting TM 2 and 3 (two of five mutants) or Y248H in the C-terminal, cytoplasmic tail region (three of five mutants) (Figure 10a). We then performed targeted mutagenesis to generate the corresponding *motA* variants in wild type,  $\Delta motF$ , and  $\Delta fliL$  background strains and performed quantitative swim ring analyses. As was reported for the original

suppressor mutants, the  $\Delta motF motA_{G136S}$  and  $\Delta motF motA_{Y248H}$  double mutant strains exhibited partially restored swimming on soft agar with an average swim ring diameter of about 20–25% of wild type (compared to about 5% for the  $\Delta motF$  mutant; Figure 11a). The percentage of motile  $\Delta motF motA_{G136S}$  and  $\Delta motF motA_{Y248H}$  mutant cells was twice that of the  $\Delta motF$  parental strain (from  $2.1 \pm 0.5\%$  to  $3.5 \pm 1.8$  and  $5.5 \pm 2.5$ , respectively), and the average swimming

TABLE 2 Quantification of motile populations and swimming velocities of *S. meliloti* wild type and mutant strains

Strain	Percent motile	Swimming velocity ( $\mu\text{m/s}$ )
WT	$36.0 \pm 8.2$	$37.7 \pm 1.7$
$motA_{G136S}$	$18.4 \pm 1.9$	$37.3 \pm 0.8$
$motA_{Y248H}$	$21.1 \pm 4.0$	$37.4 \pm 1.6$
$motB_{K60A}$	$25.0 \pm 8.9$	$36.3 \pm 0.7$
$motB_{A64E}$	$22.8 \pm 10.6$	$38.7 \pm 1.6$
$motB_{\Delta\text{plug}}$	$16.4 \pm 6.5$	$19.9 \pm 2.0$
$\Delta motF$	$2.1 \pm 0.5$	$10.9 \pm 0.6$
$\Delta motF motA_{G136S}$	$3.5 \pm 1.8$	$13.1 \pm 0.4$
$\Delta motF motA_{Y248H}$	$5.5 \pm 2.5$	$12.4 \pm 1.3$
$\Delta motF motB_{K60A}$	$5.3 \pm 1.2$	$13.9 \pm 1.6$
$\Delta motF motB_{A64E}$	$9.3 \pm 3.8$	$16.7 \pm 1.1$
$\Delta motF motB_{\Delta\text{plug}}$	$10.7 \pm 4.9$	$17.4 \pm 1.2$
$\Delta flil$	Nonmotile	Nonmotile
$\Delta flil motA_{G136S}$	Nonmotile	Nonmotile
$\Delta flil motA_{Y248H}$	Nonmotile	Nonmotile
$\Delta flil motB_{K60A}$	Nonmotile	Nonmotile
$\Delta flil motB_{A64E}$	$0.2 \pm 0.2$	$8.8 \pm 1.4$
$\Delta flil motB_{\Delta\text{plug}}$	$0.4 \pm 0.2$	$7.7 \pm 1.9$

velocity was marginally improved (Table 2). Furthermore, both mutants exhibited increased average rotational velocity in tethered cell experiments compared to the wild type (Figure 12a). However, neither of the  $motA$  second-site mutations conferred motility to the  $\Delta flil$  parental strain on swim plates or in the motility medium (Figure 11a and Table 2). Finally, the respective  $motA$  point mutations in the wild-type background elicited no effect on motility (Figures 11a and 12a, Table 2).

It has been previously reported that point mutations in the plug region of MotB can partially restore motility of  $\Delta flil$  strains in *R. sphaeroides* and *S. typhimurium*, namely F63L and A67D/E, and L56A and A60E, respectively. A multiple sequence alignment using T-Coffee identified equivalent residues in *S. meliloti* MotB as K60 and A64 (Figure 10b). Thus, we created similarly disruptive mutations by introducing either a neutralizing (K60A) or a negatively charged (A64E) residue in wild-type,  $\Delta motF$ , and  $\Delta flil$  backgrounds. Additionally, we asked whether the removal of the entire MotB plug region (corresponding to residues 58–69) would influence motility. All three strains with mutations in the plug region, specifically  $motB_{K60A}$ ,  $motB_{A64E}$ , and  $motB_{\Delta\text{plug}}$ , referred to here as  $motB_{\text{plug}}$  mutants, restored the motility of  $\Delta motF$  on swim plates to about 20% of wild type, similar to the  $motA$  second-site mutants (Figure 11b). The percentage of motile cells (5%) and average swimming speed ( $13.9 \mu\text{m/s}$ ) were similarly improved for  $\Delta motF motB_{K60A}$  (Table 2). However, the introduction of  $motB_{A64E}$  and  $motB_{\Delta\text{plug}}$  into  $\Delta motF$  resulted in an even greater enhancement of the percentage of motile cells (~10%) and swimming velocity of the motile population (~17  $\mu\text{m/s}$ ). All 3 second-site mutations in the  $\Delta motF$  background caused improved tethered cell rotation rates compared to the  $\Delta motF$  parent strain (Figure 12b). The introduction of  $motB_{\Delta\text{plug}}$  resulted in the greatest improvement with an average rotation rate of 4.1 Hz. In contrast,  $motB$  plug mutations in the  $\Delta flil$  background did not permit swimming on soft agar plates. The  $\Delta flil motB_{A64E}$  and  $\Delta flil$

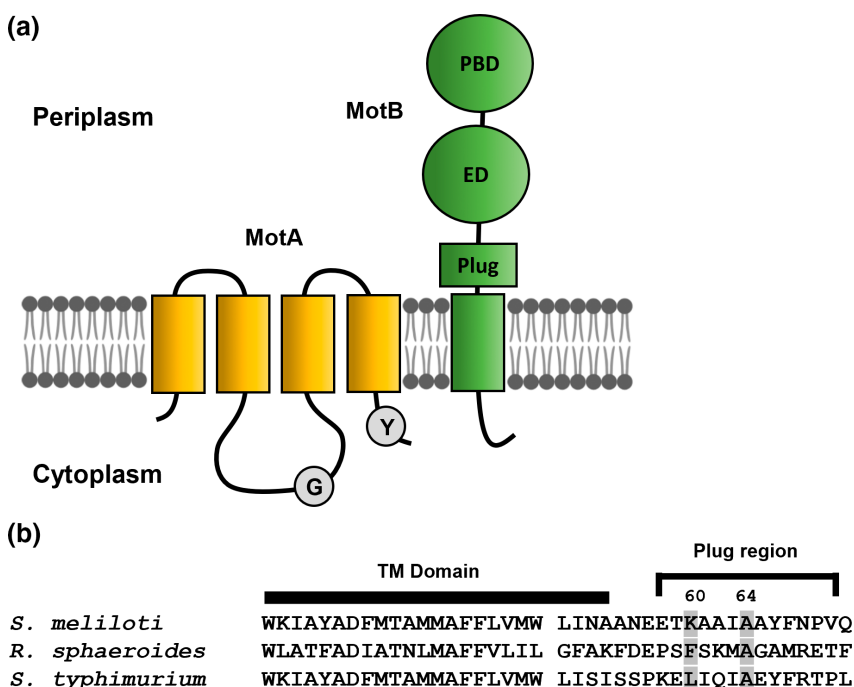
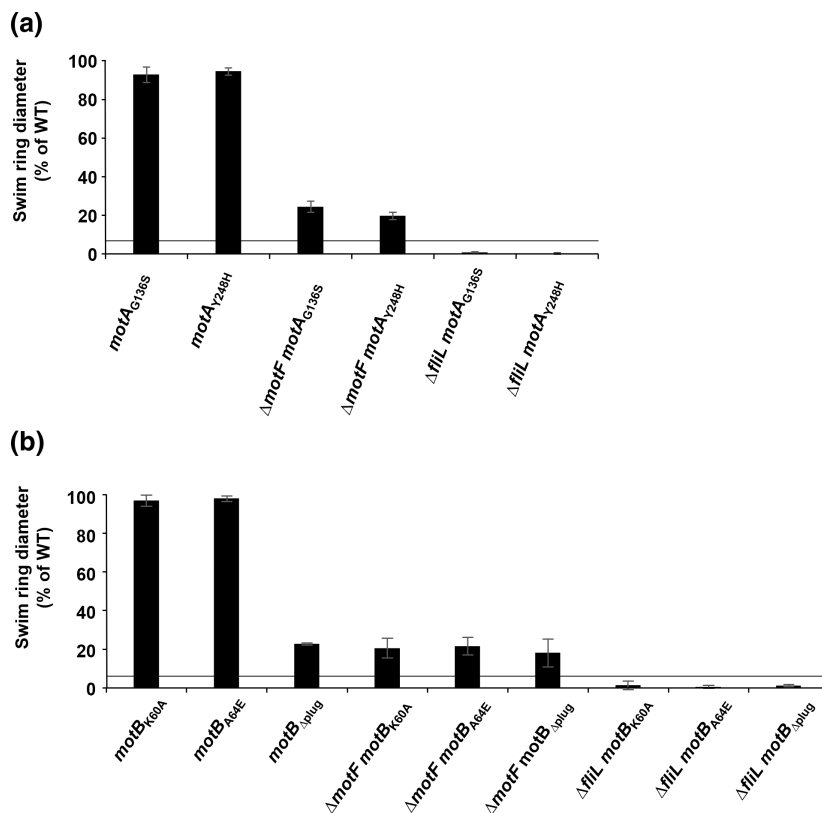


FIGURE 10 Topology and sequence alignment of stator proteins. (a) Topology of MotA and MotB marking the position of mutated residues. G, Gly136; Y, Tyr248; PBD, peptidoglycan binding domain; ED, *S. meliloti* extra domain; plug, MotB plug region (aa 58–69) (b) multiple sequence alignment of the N-terminal region of *S. meliloti*, *R. sphaeroides*, and *S. typhimurium* MotB using the T-coffee server (Magis et al., 2014). MotB TM domains are indicated by a black line and the plug regions are bracketed. The position of mutated residues is labeled with the corresponding *S. meliloti* MotB amino acid residue number.

**FIGURE 11** Swim ring analysis of  $\Delta motF$  and  $\Delta fliL$  strains with second-site mutations in *motA* (a) and *motB* (b). Horizontal black lines serve as a reference of the  $\Delta motF$  swim ring diameter. Data are averages and standard deviations for at least three independent experiments with three technical replicates.



*motB*<sub>Δplug</sub> mutants exhibited a very small degree of swimming ability (<0.5% motile and swimming velocities of <9  $\mu\text{m/s}$ ), albeit still inferior to the  $\Delta motF$  mutant. It should be noted that the introduction of the *motB*<sub>Δplug</sub> mutation in the wild-type background reduced motility in all assays (Figures 10 and 11, and Table 2). Altogether, these data suggest that mutations that disrupt the MotB proton channel plug can partially bypass the requirement for MotF in flagellar motor function but not for FliL, and by extension that MotF is required for proton plug modulation.

### 3 | DISCUSSION

#### 3.1 | MotF and FliL: Paralogous proteins required to drive the flagellar motor

In this work, we provide the first report of a novel FliL paralog, MotF, operating in conjunction with FliL to drive motor rotation. Our motility analyses demonstrate that MotF and FliL are both essential to support flagellar motor function in *S. meliloti*. The presence of two *fliL* copies has been described for bacterial species that employ more than one type of flagellar system, such as *V. alginolyticus*, *Bradyrhizobium diazoefficiens*, and *Shewanella putrefaciens* (Lin et al., 2018; Mengucci et al., 2020; Pecina et al., 2021). However, in all of these cases, the two FliL paralogs are part of separate flagellar systems, specifically a lateral multi-flagellar system or a single (sub) polar flagellum. In contrast, *S. meliloti* is only known to possess one flagellar system, and thus we explored the specific roles of the two

FliL paralogs employed within their peritrichous flagella. Our combined experimental evidence suggests co-dependence of MotF and FliL and closely linked functions: (1) MotF and FliL levels are reduced in deletion mutants of *fliL* and *motF*, respectively; (2) both proteins interact with each other in BACTH and pull-down assays; (3) strains lacking *motF* or *fliL* exhibit severe flagellar motor impairment.

#### 3.2 | Roles of MotF and FliL in flagellation

While the  $\Delta motF$  mutant retained flagella at wild-type levels and quality, transmission electron microscopy analysis showed that the  $\Delta fliL$  mutant was mostly aflagellate and transcriptional and immunoblot analyses revealed reduced flagellin production. The inability to produce functional filaments negatively regulates the promoter activity of the principal flagellin gene *flaA* in a feedback mechanism (Scharf et al., 2001). We can only speculate how FliL contributes to the production and/or stabilization of *S. meliloti* flagellar filaments. Reduced flagellation in the absence of *fliL* has been reported previously in *Pseudomonas putida* (Segura et al., 2001) and *Silicibacter* sp. strain TM1040 (Belas et al., 2009). A *Salmonella fliL* mutant exhibits a rod-breakage phenotype under swarming conditions implying a role for FliL in rod stability under high load (Attmannspacher et al., 2008; Partridge et al., 2015). However, we determined that the reduced flagellin levels of the *S. meliloti*  $\Delta fliL$  mutant were not restored by paralyzing the flagellar motor indicating that the reduced flagellin production by this mutant is unlikely to be caused by reduced rod stability during filament rotation.



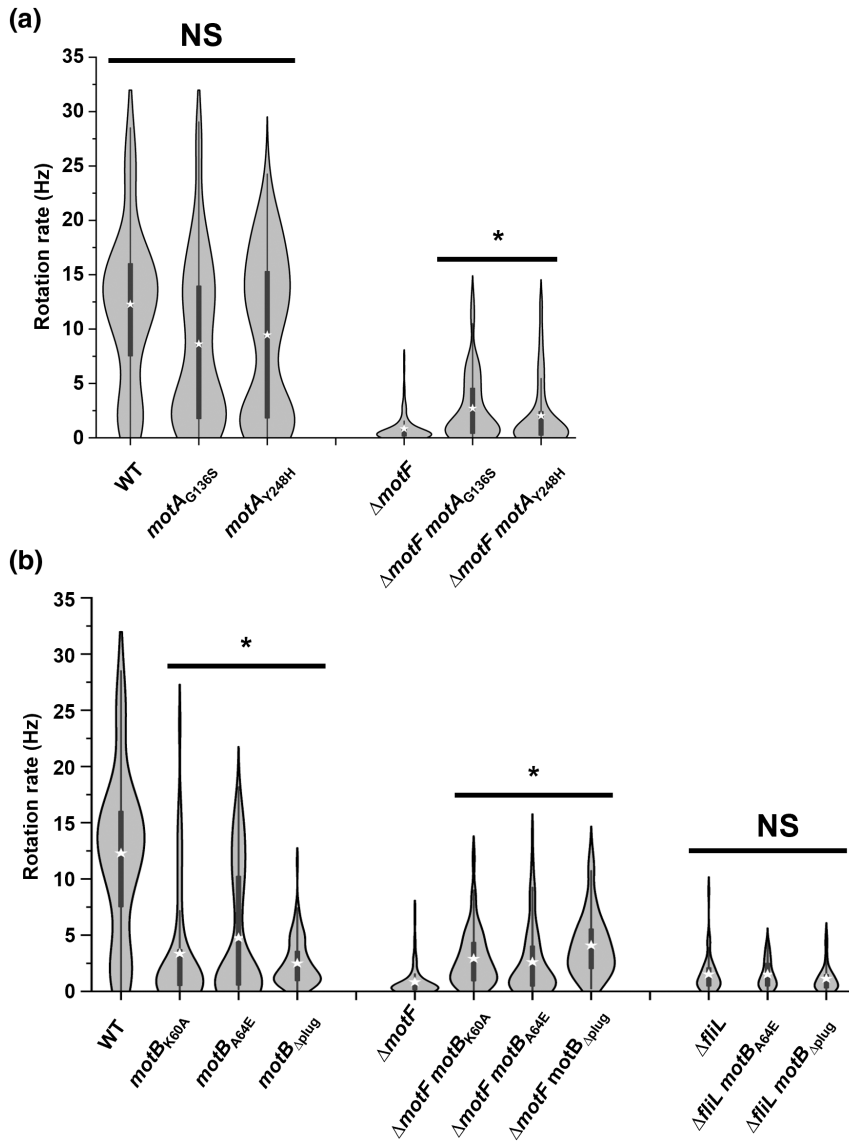


**FIGURE 12** Flagellar motor behavior of  $\Delta motF$  and  $\Delta fliL$  strains with mutations in *motA* (a) and *motB* (b) in the tethered-cell assay. Tethered cell rotation rates of wild type (WT) and *mot* mutants ( $n = 100$  each for wild-type and  $\Delta motF$  background strains and  $n = 40$  for  $\Delta fliL$  background strains). Dots indicate average rotation rates and boxes correspond to the interquartile ranges. Asterisks indicate a significant difference of the means ( $p > .02$ ) from the corresponding parental strain as determined by the Kruskal-Wallis and Dunn's multiple comparisons post hoc tests. NS, not significant.

In contrast to *Salmonella* and *E. coli*, the lack of *fliL* in *P. mirabilis* caused a more pronounced swimming defect, and swarming was only affected in a temperature-dependent manner (Lee & Belas, 2015). Additionally, while *P. mirabilis* wild-type cells require 1.5% agar for swarmer differentiation,  $\Delta fliL$  mutant cells also swarm on 0.9% agar, suggesting a role of FliL in surface sensing-dependent differentiation (Lee & Belas, 2015). Thus, FliL in *P. mirabilis* is not a rod-reinforcement module as seen in swarming *Salmonella*. To add to the variable function of FliL, cells of *C. crescentus* (Jenal et al., 1994), *R. sphaeroides* (Suaste-Olmos et al., 2010), as well as swimming *Salmonella* (Attmannspacher et al., 2008) exhibit normal flagellation in the absence of *fliL*. Thus, *S. meliloti* MotF would be appropriately placed in the FliL-class described above. Another phenotype has been observed in *B. burgdorferi*, in which the lack of FliL caused a decrease in swimming velocity due to misorientation of 50% of its internal flagella (Motaleb et al., 2011). In summary, while FliL proteins in various bacterial species exhibit some unifying characteristics as they are linked to flagellar motor performance, their functions are numerous and appear to be largely species-specific.

### 3.3 | Importance of MotF and FliL in torque generation and MotB plug function

The *motF* and *fliL* deletion strains both exhibited very poor motor performance in tethered cell experiments. However, it was much more difficult to find examples of rotating  $\Delta fliL$  cells, an observation that may be explained by strongly diminished flagellation and/or further impairment of motor function. In accordance with these observations, the  $\Delta fliL$  mutant was completely nonmotile and less than 1% of cells were found to twirl in place. Although  $\Delta motF$  cells were mostly nonmotile, about 2% of bacteria (compared to 36% motile for the wild type) retained some degree of slow and jerking swimming motility.

We isolated suppressor mutants with partially restored swimming ability after extended incubation of the  $\Delta motF$  strain on soft agar. The two unique SNPs in *motA*, *motA*<sub>G136S</sub>, and *motA*<sub>Y248H</sub>, when introduced into *S. meliloti* wild type, had little effect on motility, but improved overall swimming population, swimming velocity, and tethered cell rotation rates of the  $\Delta motF$  strain. The same mutations

were unable to restore motility of the  $\Delta$ *fliL* strain, which is supporting evidence for distinct functions of MotF and FliL. Intriguingly and despite multiple attempts, we have not been able to obtain suppressor mutants for the  $\Delta$ *fliL* strain, suggesting that *S. meliloti* FliL is indispensable for flagellar function and swimming motility.

Specific second-site mutations in the MotB plug region restore motility defects in *R. sphaeroides* (Suaste-Olmos et al., 2010) and *S. enterica* (Partridge et al., 2015)  $\Delta$ *fliL* mutants. Thus, we tested whether comparable mutations in *S. meliloti* MotB<sub>plug</sub> would similarly improve the *fliL* or *motF* deletion phenotypes. We saw no such restoration for the  $\Delta$ *fliL* mutant, other than a minimal increase in the number of cells with motility reminiscent of the  $\Delta$ *motF* mutant. However, disruption of the MotB proton channel plug greatly improved the swimming and flagellar motor rotation defects of the  $\Delta$ *motF* mutant as did deletion of the entire MotB plug. Motility phenotype restoration was comparable to that of the *motA* second-site mutants suggesting that the latter modifications may distort the proton channel sufficiently to mimic the removal of the MotB plug region.

In addition to its role in MotB<sub>plug</sub> modulation, FliL has been linked to the stomatin/prohibitin/flotillin/HflK/C (SPFH) family of scaffolding proteins (Takekawa et al., 2019). In *R. sphaeroides* and *S. enterica*, it was shown that FliL associates with basal body components (Partridge et al., 2015; Suaste-Olmos et al., 2010). Additionally, the localization of *V. alginolyticus* MotAB stator units at the basal body is reduced in the absence of FliL (Lin et al., 2018). From these findings, coupled with our behavioral data, we speculate that *S. meliloti* FliL may serve as an essential primary scaffold at the flagellar basal body, which stators may assemble onto and become stabilized. Then, MotF may assemble around the stators to unlock the MotB<sub>plug</sub> from its inactive state within the periplasmic crenulations of pentameric MotA and modulate the MotB<sub>plug</sub> region. This hypothesis is in line with the observations that (1) FliL is essential, (2) the absence of MotF can be overcome by removing the MotB<sub>plug</sub>, and (3) removal of the MotB<sub>plug</sub> is equally detrimental as the loss of MotF.

Partridge et al. proposed that FliL may either increase stator occupancy or alternatively increase the dwell time of stators at the motor (Partridge et al., 2015). Based on the tethering results reported here, both hypotheses are plausible for *S. meliloti* MotF and FliL. Clearly, MotF is directly and FliL directly or indirectly required for torque generation in *S. meliloti* as has been observed for FliL in other alphaproteobacteria including *R. sphaeroides* and *C. crescentus* and the lateral flagellar system of *B. diazoefficiens* (Jenal et al., 1994; Mengucci et al., 2020; Suaste-Olmos et al., 2010). Structural analyses have informed a model in which FliL forms a partial ring, which serves as a scaffold awaiting incoming stators before it oligomerizes into a fully encapsulating ring structure. The FliL proteins in *C. jejuni* and *B. burgdorferi* readily form such partial rings of 4–5 monomers (Guo et al., 2022; Tachiyama et al., 2022). We similarly observed dimers and trimers of the periplasmic region of MotF in chemical cross-linking experiments. Additionally, the periplasmic domain of MotB or MotC was found to promote further MotF oligomerization into high molecular weight complexes reaching up to ~250kDa, perhaps corresponding to a MotB\* or MotC dimer (~80kDa) in complex

with up to a decamer of MotF\* (185kDa). In contrast, the periplasmic regions of MotF and FliL did not interact with each other implying that their transmembrane domains (directly or indirectly) are mediating their association.

*S. meliloti* MotB contains one large (~90 aa residue) insertion in its periplasmic domain compared to *E. coli* MotB indicating the existence of additional contacts with other components of the *S. meliloti* flagellar motor. Some preliminary data point to an interaction of *S. meliloti* MotB with the alphaproteobacteria-specific MotC protein. In addition, the work presented here demonstrates interactions between MotF and FliL with MotB and MotA and provided evidence for a MotF/MotC interaction. We propose that MotF is the primary MotB<sub>plug</sub> modulator, while FliL and/or MotC engage with this additional MotB region.

### 3.4 | Model and concluding remarks

Altogether, these data lead to a model where partial rings of *S. meliloti* FliL and MotF assemble at the basal body prior to stator incorporation (Figure 13). As stators engage the basal body/FliL/MotF complex, additional FliL and MotF proteins complete their rings to stabilize the stators and modulate the MotB plug region. In the absence of either of these proteins, stator assembly and torque generation are drastically reduced. For motors without the FliL scaffold, stator assembly is nearly abolished, whereas motors lacking MotF can achieve stator incorporation by FliL, although the MotB plug remains primarily in the inactive state resulting in slow or no motor rotation.

Why would *S. meliloti* employ two distinct proteins to do the job that one can accomplish in other bacteria? This may be driven by the distinct motility behavior of this organism: *S. meliloti* employs unidirectional speed-variable motors whereas many other characterized bacteria use variations on the reversible switch type-motor theme. *S. meliloti* is also capable of effectively swimming in environments of higher viscosity, which is mediated by the screw-like surface structure of its flagellar filaments (Götz et al., 1982; Kreutzberger et al., 2022; Trachtenberg et al., 1986). These adaptations may require additional motor components, such as MotF and MotC. It would also be interesting to explore the architecture of the *S. meliloti* flagellar motor in light of the intricacy and diversity of basal body structures from distantly related organisms (Chen et al., 2011; Deme et al., 2020; Ferreira et al., 2019; Guo et al., 2022; Hu et al., 2021; Johnson et al., 2021; Kojima et al., 2018; Minamino & Imada, 2015; Rossmann et al., 2020; Santiveri et al., 2020; Tachiyama et al., 2022; Takekawa et al., 2019; Terashima et al., 2017). It is intriguing to speculate how exactly MotF and FliL are arranged in the *S. meliloti* flagellar motor. Do they form stacked or concentric rings around the stators? It also remains to be determined how MotC fits into the structure and function of the *S. meliloti* flagellar motor. How is rotational speed modulated and how is the motor locked into a clockwise rotation? These questions and more will be the focus of future studies as we dissect the mechanisms driving the function of this macromolecular marvel.

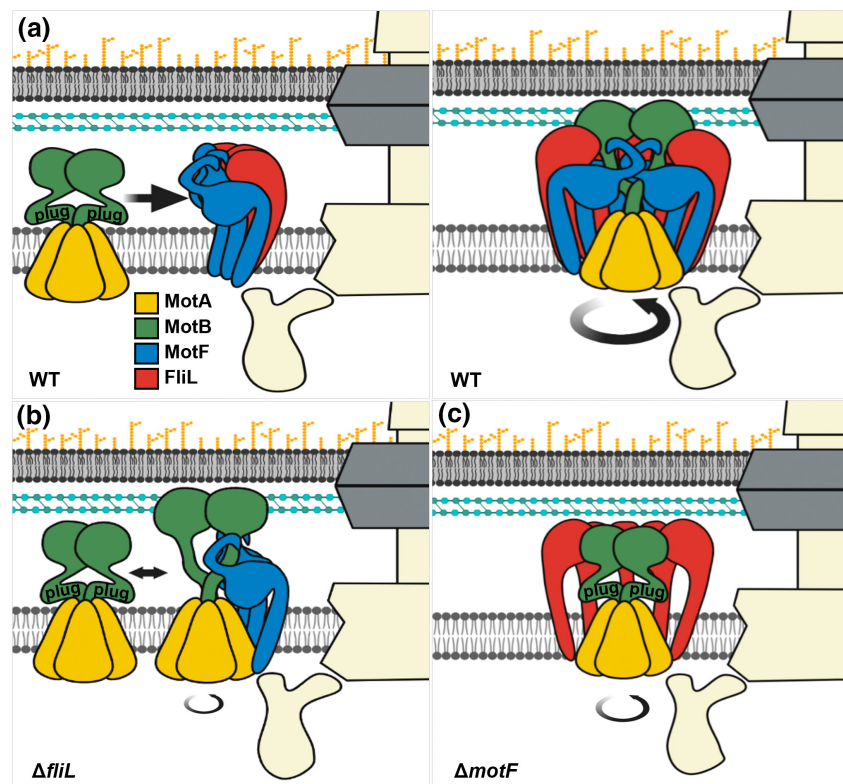


**FIGURE 13** Model describing the roles of MotF and FliL and effects of their absence on flagellar motility in *S. meliloti*. (a) in the wild type, stator units are recruited to basal bodies by partial rings of FliL and MotF (top left panel), which recruit additional FliL and MotF proteins to form a cage around the stators. MotF modulates the MotB<sub>plug</sub> to promote motor rotation (top right panel). (b) in the absence of MotF, stators are stabilized by FliL near the basal body but are unable to release MotB<sub>plug</sub>, resulting in overall low torque generation. (c) in motors without FliL, stators associate with MotF but remain unable to securely integrate into the basal body leading to low torque generation. The hook-like extension on MotF represents the additional ~40 aa region present on MotF proteins that is absent from FliL proteins.

## 4 | EXPERIMENTAL PROCEDURES

### 4.1 | Strains and plasmids

Derivatives of *E. coli* K-12, highly motile derivatives of *S. meliloti* MVII-1, and the plasmids used in this study are described in Table S4.

### 4.2 | Media and growth conditions

*E. coli* strains used for IMPACT protein purification, pull-down assays, or bacterial two-hybrid (BACTH) analyses were grown in lysogeny broth (LB; [Bertani, 1951]) at 37°C or 30°C with appropriate antibiotics at the following concentrations: ampicillin (Ap) at 100 µg/ml and kanamycin (Km) at 50 µg/ml.

*S. meliloti* strains were routinely grown in tryptone-yeast extract-calcium chloride (TYC) medium supplemented with streptomycin (Sm; 600 µg/ml) at 30°C (Baaziz et al., 2021). For motility assays, stationary phase cultures were diluted to an OD<sub>600</sub> of 0.01 and grown for 24 h. Cultures were diluted to an OD<sub>600</sub> of 0.004 in 10 ml Rhizobium basal medium (RB) [6.1 mM K<sub>2</sub>HPO<sub>4</sub>, 3.9 mM KH<sub>2</sub>PO<sub>4</sub>, 1 mM MgSO<sub>4</sub>, 1 mM (NH<sub>4</sub>)<sub>2</sub>SO<sub>4</sub>, 0.1 mM CaCl<sub>2</sub>, 0.1 mM NaCl, 0.01 mM Na<sub>2</sub>MoO<sub>4</sub>, 0.001 mM FeSO<sub>4</sub>, 20 mg/L biotin, and 100 mg/L thiamine] on Bromfield plates and grown at 30°C for 16 h to an OD<sub>600</sub> of 0.25 ± 0.05 (Bromfield overlay plates) (Baaziz et al., 2021). Antibiotics for *S. meliloti* strains bearing plasmids were provided at the following concentrations: neomycin at 120 µg/ml and tetracycline at 10 µg/ml.

### 4.3 | Swim plate assays

Swim plates (0.3% agar) containing Bromfield medium (0.04% Bacto tryptone, 0.01% yeast extract, 0.01% CaCl<sub>2</sub>, 0.3% agar) were inoculated with 3 µl of stationary-phase cultures and incubated for 3–5 days at 30°C.

### 4.4 | Cell fractionation

Bacterial cells from 20 Bromfield overlay plates were harvested by centrifugation at 5000g for 10 min at 4°C. Samples were kept on ice/at 4°C for the remainder of the experiment. Bacteria were suspended in C-buffer (10 mM MgCl<sub>2</sub>, 50 µg/ml DNase A, 50 µg/ml RNase I, 20 mM Tris/HCl, pH 8.0) and lysed by three passages through a mini-French pressure cell at 14,000 lb/in<sup>2</sup> (SLM Aminco, Silver Spring, MD). Unlysed cells were removed by centrifugation for 5 min at 15,000g and the supernatants were recovered. Membranes were pelleted at 160,000g for 90 min at 4°C, and the supernatants were retained as soluble fractions. Membranes were washed once in C-buffer and suspended in Laemmli buffer. All samples were boiled for 10 min prior to SDS-PAGE and immunoblotting.

### 4.5 | Purification of recombinant proteins

Periplasmic domains of MotF (MotF\*), MotB (MotB\*), FliL (FliL\*), and mature MotC (MotC\*) were expressed from pBS357, pBS56,

pBS1286, and pBS54, respectively, in *E. coli* ER2566 (Table S4) using the Intein-Mediated Purification with an Affinity Chitin-binding Tag (IMPACT™) method as described previously (Mitchell & Lorsch, 2015). Briefly, cells were grown to an OD<sub>600</sub> of 0.5 to 0.7 at 37°C in LB broth and expression was induced by the addition of 0.3 mM isopropyl β-D-1-thiogalactopyranoside (IPTG) and incubation overnight at 16°C. Cells were harvested at 16,000g for 10 min at 4°C, suspended in IMPACT buffer (20 mM Tris-HCl, 500 mM NaCl, 1 mM EDTA, 1 mM phenylmethylsulfonyl fluoride [PMSF], pH 8.0) and lysed by three passages through a French pressure cell at 14,000 lb/in<sup>2</sup>. Cell debris was removed by centrifugation at 56,000g for 90 min at 4°C and the soluble fraction was loaded onto a gravity flow column containing a 25-ml bed of chitin-agarose that was pre-equilibrated with IMPACT buffer. Cleavage was performed by addition of IMPACT buffer supplemented with 50 mM dithiothreitol and continued incubation at 4°C for 40 h, and cleaved proteins were eluted with IMPACT buffer. Proteins were concentrated in an Amicon ultrafiltration apparatus with a regenerated 10 kDa MWCO cellulose membrane and further purified by fast-performance liquid chromatography at 1 ml/min using a HiPrep 26/60 Sephacryl S-200 HR column (Cytiva) equilibrated in cross-linking buffer (150 mM NaCl, 20 mM sodium phosphate, 5% [w/v] glycerol, pH 8.0). Fractions containing target proteins were concentrated as described above and protein concentrations were determined by the Bradford protein assay (Bio-Rad) prior to use in cross-linking experiments.

#### 4.6 | In-vitro cross-linking experiments

Purified proteins at a concentration of 10 μM were incubated in cross-linking buffer (150 mM NaCl, 20 mM sodium phosphate, 5% [w/v] glycerol, pH 8.0) in the presence or absence of 10 mM glutaraldehyde for 1 h prior to quenching with an equal volume of Laemmli buffer. Reaction mixtures were boiled at 100°C for 10 min and analyzed by immunoblotting.

#### 4.7 | SDS-PAGE and immunoblotting

When necessary, polyclonal antibodies were affinity-purified as described previously (Scharf et al., 2001). One-ml culture aliquots grown in Bromfield overlay plates were pelleted at 15,000g and all but ~15 μl of the supernatants were removed. Cells were suspended in the remaining supernatant and 15 μl Laemmli buffer was added prior to boiling for 10 min. For *S. meliloti* flagellin immunoblots, 15 μl of cell culture were mixed with 15 μl of Laemmli buffer and boiled for 10 min. All samples were stored frozen at -20°C until further processing. Immunoblot analysis was performed essentially as described previously (Zatakia et al., 2018) except that four washes were used after each antibody incubation. Primary antibodies were used in blocking buffer (PBS supplemented with 5% [w/v] skim milk) at the following concentrations: polyclonal rabbit anti-flagellin,

-MotF, -FlilL crude sera were used at 1:10,000; affinity-purified anti-MotB, -MotC, -MotE, and -CheR antibodies were used at 1:100, 1:67, 1:200, and 1:1000, respectively, and monoclonal mouse anti-6x-His antibody (Santa Cruz Biotech, Santa Cruz CA) was used at 1:50. Donkey anti-rabbit HRP secondary antibody (NA-934, Cytiva) was used at 1:10,000 and anti-mouse HRP (NXA-931, Cytiva) was used at 1:1000.

#### 4.8 | Bacterial two-hybrid analysis

Triplicate LB-Ap-Km cultures were prepared from single colonies in LB broth and grown overnight at 30°C. Four microliters of stationary-phase cultures were spot-inoculated on MacConkey/lactose agar (Difco) plates supplemented with ampicillin and kanamycin (Battesti & Bouveret, 2012). Positive interactions were identified as colonies yielding red color after a 48-h incubation period at 30°C. Representative results from three independent experiments were reported.

#### 4.9 | Membrane topology reporter assay

MotF topology was investigated using a transcriptional fusion of *phoA* and *lacZα* to the 3' end of *motF* or the 3' end of the MotF transmembrane domain-encoding region in the reporter plasmid pKTop (Karimova et al., 2009; Karimova & Ladant, 2017). *E. coli* DH5α was transformed with the resulting plasmids, pBS1319 and pBS1320, and single colonies were streaked on LB agar plates supplemented with 1 mM IPTG and 80 μg/ml 5-chloro-4-bromo-3-indolyl phosphate (X-Phos) (RPI, Mt Prospect, IL, USA) and incubated overnight at 30°C. Strains harboring pKTop or pKTop encoding a C-terminal fusion of the first 39 amino acids of YmgF (Karimova et al., 2009) served as a negative and positive control for cytoplasmic or periplasmic localization, respectively.

#### 4.10 | β-Galactosidase assays

Stationary cultures of co-transformed *E. coli* BTH101 Δ*flhC* strains were diluted 1:100 in LB broth and grown to an OD<sub>600</sub> of 1.6 ± 0.2. An appropriate amount of culture was collected and stored at -20°C. Z-buffer (60 mM Na<sub>2</sub>HPO<sub>4</sub>, 40 mM NaH<sub>2</sub>PO<sub>4</sub>, 10 mM KCl, 1 mM MgSO<sub>4</sub>, 50 mM β-mercaptoethanol, pH 7.0) was added to obtain a final volume of 1 ml prior to addition of 30 μl chloroform and 30 μl of 0.1% SDS. Samples were vortexed vigorously for 10 sec and incubated for five min at 28°C. Two hundred microliters of 4 mg/ml O-nitrophenyl-β-D-galactoside (ONPG) was added, and reactions were continued until a faint yellow appearance was observed and stopped by the addition of 500 μl 1 M Na<sub>2</sub>CO<sub>3</sub>. Samples were centrifuged at 21,000g for two min and the absorbance at 420 nm of the supernatants was recorded. The relative β-galactosidase activity was expressed in Miller units and determined using the formula:

$(1000) \cdot (A_{420}) / (\Delta t \cdot v \cdot OD_{600})$ , where  $\Delta t$  is the reaction duration and  $v$  is the culture volume in milliliters in the reaction. Reported values are the averages and standard deviations of three experiments each performed in triplicate. Cultures of *S. meliloti* containing *pflA-lacZ* fusions were sampled, diluted 1:1 in Z buffer (Miller, 1972), permeabilized with 30  $\mu$ l chloroform and 30  $\mu$ l 0.1% SDS, and assayed for  $\beta$ -galactosidase activity as described above.

#### 4.11 | Pull-down assays

Overnight cultures of *E. coli* BL21 (DE3) with pETDuet-1 derivatives (Table S4) were diluted 1:1000 in LB broth and grown at 37°C to an  $OD_{600}$  of 0.5 to 0.7 prior to induction with 0.3 mM IPTG for 4 h at 25°C. Aliquots of 70 ml were harvested by centrifugation at 16,000g for 5 min at 4°C and stored at -20°C. Cell pellets were thawed and suspended in 2 ml Ni-NTA MagBeads prewashed with binding buffer (20 mM sodium phosphate, 500 mM NaCl, 20 mM imidazole, 0.4% CHAPS (3-[[3-cholamidopropyl]-dimethylammonio]-1-propanesulfonate), 1 mM PMSF, 1 mg/ml lysozyme, and 5  $\mu$ g/ml DNase I pH 7.4). Cells were incubated on a rotisserie incubator for 1 h at 4°C and lysed by two passages through a mini-French pressure cell at 14,000 lb/in<sup>2</sup> (SLM Aminco, Silver Spring, MD). Unlysed cells and insoluble debris were removed by centrifugation at 16,000g for 45 min at 4°C. PureCube Ni-NTA MagBeads (Cube Biotech, Monheim am Rhein, Germany) were prepared by washing 20  $\mu$ l resin slurry thrice with 1 ml binding buffer. Soluble fractions were mixed with the washed resin and incubated on a rotisserie incubator for 1 h at 4°C. The unbound fraction was removed and the resin was washed four times each with 200  $\mu$ l binding buffer without CHAPS. Bound proteins were eluted twice by the addition of 50  $\mu$ l elution buffer (20 mM sodium phosphate, 500 mM NaCl, 500 mM imidazole, pH 7.4). Samples of the soluble fraction (200 ng of total protein) and elution fraction (25 ng of total protein) were analyzed by immunoblotting as described above.

#### 4.12 | Computerized swimming and cell tethering analysis

Bacteria were grown on Bromfield overlay plates to an  $OD_{600}$  of  $0.25 \pm 0.05$ , harvested by centrifugation at 4000g for 8 min at room temperature, and suspended in overlay broth that was prepared by incubating Bromfield plates with a 10-ml layer of RB at 30°C for 16 h and passing the supernatant through a 0.22  $\mu$ m PES filter. To assess the percentage of motile cells and determine swimming velocities, bacteria were adjusted to an  $OD_{600}$  of 0.05 and analyzed by phase-contrast microscopy using a Nikon Eclipse E600 microscope with a 40x objective and a custom Nikon CMOS camera from The Imaging Source (Charlotte, NC, USA). Five-second videos were analyzed using the TumbleScore program to quantify swimming velocities (Pottash et al., 2017). For quantification of percent motile bacteria, the videos were shortened to 2 s, and the number of motile bacteria was

determined. The two-second videos were reanalyzed with the "stuck distance" setting—corresponding to the distance a bacterium must move in a trajectory to be considered not stuck—reduced to zero and the number of bacteria in the video was counted. The percentage of motile bacteria was calculated by dividing the number of motile bacteria by the total bacteria in the two-second videos. For tethering analyses, chloramphenicol (Cp) was added at a final concentration of 30  $\mu$ g/ml to 2 ml of cell suspension standardized to an  $OD_{600}$  of 0.20 and incubated at room temperature for 20 min. Flagella were sheared by 15 passages through syringes equipped with 26-gauge beveled needles attached by plastic tubing. Cells were pelleted by centrifugation at 3000g for 6 min at room temperature and washed in 1 ml of overlay broth supplemented with Cp to remove sheared flagella. Cells were suspended in 500  $\mu$ l overlay broth with Cp and tethering to glass coverslips was achieved by incubating 10  $\mu$ l of cell suspension with 10  $\mu$ l anti-flagellin antibody (Scharf et al., 2001) diluted 1:1000 in overlay broth with Cp for 30 min at room temperature. Coverslips were inverted and fixed to glass slides with three layers of tape on either side and thin strips of Apeizon M grease. Unattached cells were removed by several washes of 100  $\mu$ l overlay broth with Cp through the channel between the slide-tape-coverslip assembly and visualized under a 100x objective lens using a Nikon Eclipse microscope equipped with a custom Nikon CMOS camera. Tethered cell rotation rates were quantified using custom scripts written in MATLAB.

#### 4.13 | Transmission electron microscopy

Motile cells (30 ml) were harvested at an  $OD_{600}$  of  $0.25 \pm 0.05$  by centrifugation over Fluorolube® at 7000g for 10 min at room temperature. The supernatant was removed and cells were washed twice with 15 ml overlay broth over Fluorolube®. The majority of the supernatant was removed and the concentrated layer of cells (~1000  $\mu$ l) on top of the Fluorolube® layer was collected. A sample was observed by phase-contrast microscopy to ensure motility. Cells were fixed through the addition of 4% glutaraldehyde (diluted from a 50% stock solution in overlay broth) to a final concentration of 2% and stored at 4°C until further processing. Cells were stained for 2 min in 1% uranyl acetate and fixed to a 200-mesh copper grid (Electron Microscopy Sciences, Hatfield, PA, USA), visualized using a JEM-1400 JEOL transmission electron microscopy equipped with a W filament at 80kV, and imaged with a Gatan Orius SC100 CCD Camera (Gatan, Pleasanton CA, USA).

#### AUTHOR CONTRIBUTIONS

RCS and BES conceived and designed this study. RCS, BES, and CG performed the experiments. LTV wrote tethered cell analysis scripts under the supervision of GA. RCS and BES analyzed the data and wrote the paper. All authors edited the paper.

#### ACKNOWLEDGMENTS

We thank Drs. Gouzel Karimova and Daniel Ladant for providing the pKTop and BACTH plasmids as well as Dr. Rasika Harshey for



providing the BTH101  $\Delta flhC$  strain. We thank the BIOL4544 class of 2012 for performing the transposon mutagenesis screen that identified the *motF* mutant motility defect. We thank Elizabeth Denson for the construction of pBS357 and purification of the MotF<sub>Peri</sub> antigen used in MotF antibody production and Sahitya Biswas for assistance with some of the motility analysis. We thank Nathalie Becerra for assistance with cell fixation and staining for TEM analysis and Daniel Shickel for assisting with some of the  $\beta$ -galactosidase assays. We also thank Dr. Michael Galperin for helpful discussions. This work was supported by the National Science Foundation, Grant/Award Number: MCB-1253234, MCB-1817652, and MCB-2128232 to BS and MCB-1715185 and IOS-1855066 to GA.

## CONFLICT OF INTEREST

The authors declare no conflict of interest.

## DATA AVAILABILITY STATEMENT

The data that support the findings of this study are available from the corresponding author upon reasonable request.

## REFERENCES

- Aldridge, P. & Jenal, U. (1999) Cell cycle-dependent degradation of a flagellar motor component requires a novel-type response regulator. *Molecular Microbiology*, *32*, 379–391.
- Aldridge, P., Karlinsey, J. & Hughes, K.T. (2003) The type III secretion chaperone FlgN regulates flagellar assembly via a negative feedback loop containing its chaperone substrates FlgK and FlgL. *Molecular Microbiology*, *49*, 1333–1345.
- Attmannspacher, U., Scharf, B.E. & Harshey, R.M. (2008) Flil is essential for swarming: motor rotation in absence of Flil fractures the flagellar rod in swarmer cells of *salmonella enterica*. *Molecular Microbiology*, *68*, 328–341.
- Attmannspacher, U., Scharf, B. & Schmitt, R. (2005) Control of speed modulation (chemokinesis) in the unidirectional rotary motor of *Sinorhizobium meliloti*. *Molecular Microbiology*, *56*, 708–718.
- Baaziz, H., Compton, K.K., Hildreth, S.B., Helm, R.F. & Scharf, B.E. (2021) McpT, a broad range carboxylate chemoreceptor in *Sinorhizobium meliloti*. *Journal of Bacteriology*, *203*(17), e00216-21.
- Battesti, A. & Bouveret, E. (2012) The bacterial two-hybrid system based on adenylate cyclase reconstitution in *Escherichia coli*. *Methods*, *58*, 325–334.
- Belas, R., Horikawa, E., Aizawa, S.-I. & Suvanasuthi, R. (2009) Genetic determinants of *Silicibacter* sp. TM1040 motility. *Journal of Bacteriology*, *191*, 4502–4512.
- Belas, R. & Suvanasuthi, R. (2005) The ability of *Proteus mirabilis* to sense surfaces and regulate virulence gene expression involves Flil, a flagellar basal body protein. *Journal of Bacteriology*, *187*, 6789–6803.
- Berg, H.C. (2003) The rotary motor of bacterial flagella. *Annual Review of Biochemistry*, *72*, 19–54.
- Bertani, G. (1951) Studies on lysogenesis I: the mode of phage liberation by lysogenic *Escherichia coli*. *Journal of Bacteriology*, *62*, 293–300.
- Blair, D.F. & Berg, H.C. (1990) The MotA protein of *E. coli* is a proton-conducting component of the flagellar motor. *Cell*, *60*, 439–449.
- Carroll, B.L. & Liu, J. (2020) Structural conservation and adaptation of the bacterial flagella motor. *Biomolecules*, *10*, 1492.
- Chang, Y., Zhang, K., Carroll, B.L., Zhao, X., Charon, N.W., Norris, S.J. et al. (2020) Molecular mechanism for rotational switching of the bacterial flagellar motor. *Nature Structural & Molecular Biology*, *27*, 1041–1047.
- Chawla, R., Ford, K.M. & Lele, P.P. (2017) Torque, but not Flil, regulates mechanosensitive flagellar motor-function. *Scientific Reports*, *7*, 1–9.
- Chen, S., Beeby, M., Murphy, G.E., Leadbetter, J.R., Hendrixson, D.R., Briegel, A. et al. (2011) Structural diversity of bacterial flagellar motors. *The EMBO Journal*, *30*, 2972–2981.
- Cusick, K., Lee, Y.-Y., Youchak, B. & Belas, R. (2012) Perturbation of Flil interferes with *Proteus mirabilis* swarmer cell gene expression and differentiation. *Journal of Bacteriology*, *194*, 437–447.
- De Mot, R. & Vanderleyden, J. (1994) The C-terminal sequence conservation between OmpA-related outer membrane proteins and MotB suggests a common function in both gram-positive and gram-negative bacteria, possibly in the interaction of these domains with peptidoglycan. *Molecular Microbiology*, *12*, 333–336.
- Deme, J.C., Johnson, S., Vickery, O., Aron, A., Monkhouse, H., Griffiths, T. et al. (2020) Structures of the stator complex that drives rotation of the bacterial flagellum. *Nature Microbiology*, *5*, 1553–1564.
- Dixit, P.D. & Maslov, S. (2013) Evolutionary capacitance and control of protein stability in protein-protein interaction networks. *PLoS Computational Biology*, *9*, e1003023.
- Eggenhofer, E., Haslbeck, M. & Scharf, B. (2004) MotE serves as a new chaperone specific for the periplasmic motility protein, MotC, in *Sinorhizobium meliloti*. *Molecular Microbiology*, *52*, 701–712.
- Fabela, S., Domenzain, C., De la Mora, J., Osorio, A., Ramirez-Cabrera, V., Poggio, S. et al. (2013) A distant homologue of the FlgT protein interacts with MotB and Flil and is essential for flagellar rotation in *Rhodobacter sphaeroides*. *Journal of Bacteriology*, *195*, 5285–5296.
- Ferreira, J.L., Gao, F.Z., Rossmann, F.M., Nans, A., Brenzinger, S., Hosseini, R. et al. (2019)  $\gamma$ -Proteobacteria eject their polar flagella under nutrient depletion, retaining flagellar motor relic structures. *PLoS Biology*, *17*, e3000165.
- Götz, R., Limmer, N., Ober, K. & Schmitt, R. (1982) Motility and chemotaxis in two strains of rhizobium with complex flagella. *Microbiology*, *128*, 789–798.
- Guo, S., Xu, H., Chang, Y., Motaleb, M.A. & Liu, J. (2022) Flil ring enhances the function of periplasmic flagella. *Proceedings of the National Academy of Sciences*, *119*, e2117245119.
- Hirano, T., Minamino, T. & Macnab, R.M. (2001) The role in flagellar rod assembly of the N-terminal domain of *salmonella* FlgJ, a flagellum-specific muramidase. *Journal of Molecular Biology*, *312*, 359–369.
- Hosking, E.R., Vogt, C., Bakker, E.P. & Manson, M.D. (2006) The *Escherichia coli* MotAB proton channel unplugged. *Journal of Molecular Biology*, *364*, 921–937.
- Hu, H., Santiveri, M., Wadhwa, N., Berg, H.C., Erhardt, M. & Taylor, N.M. (2021) Structural basis of torque generation in the bi-directional bacterial flagellar motor. *Trends in Biochemical Sciences*, *47*, 160–172.
- Imada, K. (2018) Bacterial flagellar axial structure and its construction. *Biophysical Reviews*, *10*, 559–570.
- Jenal, U., White, J. & Shapiro, L. (1994) *Caulobacter* flagellar function, but not assembly, requires Flil, a non-polarly localized membrane protein present in all cell types. *Journal of Molecular Biology*, *243*, 227–244.
- Johnson, S., Furlong, E.J., Deme, J.C., Nord, A.L., Caesar, J.J., Chevance, F.F. et al. (2021) Molecular structure of the intact bacterial flagellar basal body. *Nature Microbiology*, *6*, 712–721.
- Jumper, J., Evans, R., Pritzel, A., Green, T., Figurnov, M., Ronneberger, O. et al. (2021) Highly accurate protein structure prediction with AlphaFold. *Nature*, *596*, 583–589.
- Kaplan, M., Ghosal, D., Subramanian, P., Oikonomou, C.M., Kjaer, A., Pirbadian, S. et al. (2019) The presence and absence of periplasmic rings in bacterial flagellar motors correlates with stator type. *eLife*, *8*, e43487.
- Kaplan, M., Sweredoski, M.J., Rodrigues, J.P., Tocheva, E.I., Chang, Y.-W., Ortega, D.R. et al. (2020) Bacterial flagellar motor PL-ring disassembly subcomplexes are widespread and ancient. *Proceedings of the National Academy of Sciences*, *117*, 8941–8947.

- Karimova, G. & Ladant, D. (2017) Defining membrane protein topology using *pho-lac* reporter fusions. In: Journet, L. and Cascales, E. (Eds.) *Bacterial protein secretion systems. Methods in molecular biology*. Marseille: Institut de Microbiologie de la Méditerranée, Aix-Marseille Univ - CNRS, pp. 129–142.
- Karimova, G., Robichon, C. & Ladant, D. (2009) Characterization of YmgF, a 72-residue inner membrane protein that associates with the *Escherichia coli* cell division machinery. *Journal of Bacteriology*, *191*, 333–346.
- Kinoshita, M., Furukawa, Y., Uchiyama, S., Imada, K., Namba, K. & Minamino, T. (2018) Insight into adaptive remodeling of the rotor ring complex of the bacterial flagellar motor. *Biochemical and Biophysical Research Communications*, *496*, 12–17.
- Kojima, S., Imada, K., Sakuma, M., Sudo, Y., Kojima, C., Minamino, T. et al. (2009) Stator assembly and activation mechanism of the flagellar motor by the periplasmic region of MotB. *Molecular Microbiology*, *73*, 710–718.
- Kojima, S., Takao, M., Almira, G., Kawahara, I., Sakuma, M., Homma, M. et al. (2018) The helix rearrangement in the periplasmic domain of the flagellar stator B subunit activates peptidoglycan binding and ion influx. *Structure*, *26*, 590–598. e595.
- Kreutzberger, M.A., Sobe, R.C., Sauder, A.B., Chatterjee, S., Peña, A., Wang, F. et al. (2022) Flagellin outer domain dimerization modulates motility in pathogenic and soil bacteria from viscous environments. *Nature Communications*, *13*, 1–14.
- Krogh, A., Larsson, B., Von Heijne, G. & Sonnhammer, E.L. (2001) Predicting transmembrane protein topology with a hidden Markov model: application to complete genomes. *Journal of Molecular Biology*, *305*, 567–580.
- Kumar, A., Isumi, M., Sakuma, M., Zhu, S., Nishino, Y., Onoue, Y. et al. (2017) Biochemical characterization of the flagellar stator-associated inner membrane protein FliL from *Vibrio alginolyticus*. *The Journal of Biochemistry*, *161*, 331–337.
- Lee, Y.-Y. & Belas, R. (2015) Loss of FliL alters *Proteus mirabilis* surface sensing and temperature-dependent swarming. *Journal of Bacteriology*, *197*, 159–173.
- Lee, Y.-Y., Patellis, J. & Belas, R. (2013) Activity of *Proteus mirabilis* FliL is viscosity dependent and requires extragenic DNA. *Journal of Bacteriology*, *195*, 823–832.
- Lin, T.-S., Zhu, S., Kojima, S., Homma, M. & Lo, C.-J. (2018) FliL association with flagellar stator in the sodium-driven vibrio motor characterized by the fluorescent microscopy. *Scientific Reports*, *8*, 1–12.
- Magis, C., Taly, J.-F., Bussotti, G., Chang, J.-M., Tommaso, P.D., Erb, I. et al. (2014) T-coffee: tree-based consistency objective function for alignment evaluation. In: Lorsch, J.R. (Ed.) *Multiple sequence alignment methods*. Medical School, John Hopkins University, pp. 117–129.
- Mengucci, F., Dardis, C., Mongiardini, E.J., Althabegoiti, M.J., Partridge, J.D., Kojima, S. et al. (2020) Characterization of FliL proteins in *Bradyrhizobium diazoefficiens*: lateral FliL supports swimming motility, and subpolar FliL modulates the lateral flagellar system. *Journal of Bacteriology*, *202*, 1–15.
- Miller, J.H. (1972) *Experiments in molecular genetics*. Cold Spring Harbor: Cold Spring Harbor Laboratory Press.
- Minamino, T. & Imada, K. (2015) The bacterial flagellar motor and its structural diversity. *Trends in Microbiology*, *23*, 267–274.
- Mistry, J., Chuguransky, S., Williams, L., Qureshi, M., Salazar, G.A., Sonnhammer, E.L. et al. (2021) Pfam: the protein families database in 2021. *Nucleic Acids Research*, *49*, D412–D419.
- Mitchell, S.F. & Lorsch, J.R. (2015) Protein affinity purification using in-tein/chitin binding protein tags. In: Lorsch, J.R. (Ed.) *Methods in enzymology*. School of Medicine, John Hopkins University, pp. 111–125.
- Morimoto, Y.V., Nakamura, S., Kami-ike, N., Namba, K. & Minamino, T. (2010) Charged residues in the cytoplasmic loop of MotA are required for stator assembly into the bacterial flagellar motor. *Molecular Microbiology*, *78*, 1117–1129.
- Motaleb, M.A., Pitzer, J.E., Sultan, S.Z. & Liu, J. (2011) A novel gene in-activation system reveals altered periplasmic flagellar orientation in a *borrelia burgdorferi* fliL mutant. *Journal of Bacteriology*, *193*, 3324–3331.
- Partridge, J.D., Nieto, V. & Harshey, R.M. (2015) A new player at the flagellar motor: FliL controls both motor output and bias. *mBio*, *6*, e02367-02314.
- Pecina, A., Schwan, M., Blagotinsek, V., Rick, T., Klüber, P., Leonhard, T. et al. (2021) The stand-alone PiliZ-domain protein MotL specifically regulates the activity of the secondary lateral flagellar system in *Shewanella putrefaciens*. *Frontiers in Microbiology*, *12*, 1160.
- Platzer, J., Sterr, W., Hausmann, M. & Schmitt, R. (1997) Three genes of a motility operon and their role in flagellar rotary speed variation in *Rhizobium meliloti*. *Journal of Bacteriology*, *179*, 6391–6399.
- Pottash, A.E., McKay, R., Virgile, C.R., Ueda, H. & Bentley, W.E. (2017) TumbleScore: run and tumble analysis for low frame-rate motility videos. *BioTechniques*, *62*, 31–36.
- Raha, M., Sockett, H. & Macnab, R.M. (1994) Characterization of the fliL gene in the flagellar regulon of *Escherichia coli* and *salmonella typhimurium*. *Journal of Bacteriology*, *176*, 2308–2311.
- Rossmann, F.M. & Beeby, M. (2018) Insights into the evolution of bacterial flagellar motors from high-throughput in situ electron cryotomography and subtomogram averaging. *Acta Crystallographica Section D: Structural Biology*, *74*, 585–594.
- Rossmann, F.M., Hug, I., Sangermani, M., Jenal, U. & Beeby, M. (2020) In situ structure of the *Caulobacter crescentus* flagellar motor and visualization of binding of a CheY-homolog. *Molecular Microbiology*, *114*, 443–453.
- Rotter, C., Mühlbacher, S., Salamon, D., Schmitt, R. & Scharf, B. (2006) Rem, a new transcriptional activator of motility and chemotaxis in *Sinorhizobium meliloti*. *Journal of Bacteriology*, *188*, 6932–6942.
- Roujeinikova, A. (2008) Crystal structure of the cell wall anchor domain of MotB, a stator component of the bacterial flagellar motor: implications for peptidoglycan recognition. *Proceedings of the National Academy of Sciences*, *105*, 10348–10353.
- Santiveri, M., Roa-Eguia, A., Kühne, C., Wadhwa, N., Hu, H., Berg, H.C. et al. (2020) Structure and function of stator units of the bacterial flagellar motor. *Cell*, *183*, 244–257. e216.
- Scharf, B., Schuster-Wolff-Bühring, H., Rachel, R. & Schmitt, R. (2001) Mutational analysis of the *rhizobium lupini* H13-3 and *Sinorhizobium meliloti* flagellin genes: importance of flagellin a for flagellar filament structure and transcriptional regulation. *Journal of Bacteriology*, *183*, 5334–5342.
- Schoenhals, G.J. & Macnab, R.M. (1999) FliL is a membrane-associated component of the flagellar basal body of *Salmonella*. *Microbiology*, *145*, 1769–1775.
- Schuhmacher, J.S., Thormann, K.M. & Bange, G. (2015) How bacteria maintain location and number of flagella? *FEMS Microbiology Reviews*, *39*, 812–822.
- Segura, A., Duque, E., Hurtado, A. & Ramos, J.L. (2001) Mutations in genes involved in the flagellar export apparatus of the solvent-tolerant *Pseudomonas putida* DOT-T1E strain impair motility and lead to hypersensitivity to toluene shocks. *Journal of Bacteriology*, *183*, 4127–4133.
- Sourjik, V., Muschler, P., Scharf, B. & Schmitt, R. (2000) VisN and VisR are global regulators of chemotaxis, flagellar, and motility genes in *Sinorhizobium (rhizobium) meliloti*. *Journal of Bacteriology*, *182*, 782–788.
- Sourjik, V. & Schmitt, R. (1996) Different roles of CheY1 and CheY2 in the chemotaxis of *rhizobium meliloti*. *Molecular Microbiology*, *22*, 427–436.
- Suaste-Olmos, F., Domenzain, C., Mireles-Rodríguez, J.C., Poggio, S., Osorio, A., Dreyfus, G. et al. (2010) The flagellar protein FliL is

- essential for swimming in *Rhodobacter sphaeroides*. *Journal of Bacteriology*, 192, 6230–6239.
- Subramanian, S. & Kearns, D.B. (2019) Functional regulators of bacterial flagella. *Annual Review of Microbiology*, 73, 225–246.
- Tachiyama, S., Chan, K.L., Liu, X., Hathroubi, S., Peterson, B., Khan, M.F. et al. (2022) The flagellar motor protein FliL forms a scaffold of circumferentially positioned rings required for stator activation. *Proceedings of the National Academy of Sciences*, 119, 1–9.
- Takekawa, N., Isumi, M., Terashima, H., Zhu, S., Nishino, Y., Sakuma, M. et al. (2019) Structure of *Vibrio* FliL, a new stomatin-like protein that assists the bacterial flagellar motor function. *mBio*, 10, e00292-00219.
- Terashima, H., Kawamoto, A., Morimoto, Y.V., Imada, K. & Minamino, T. (2017) Structural differences in the bacterial flagellar motor among bacterial species. *Biophysics and Physicobiology*, 14, 191–198.
- Teufel, F., Almagro Armenteros, J.J., Johansen, A.R., Gíslason, M.H., Pihl, S.I., Tsirigos, K.D. et al. (2022) SignalP 6.0 predicts all five types of signal peptides using protein language models. *Nature Biotechnology*, 40(7), 1–3.
- Trachtenberg, S., DeRosier, D.J., Aizawa, S.-I. & Macnab, R.M. (1986) Pairwise perturbation of flagellin subunits: the structural basis for the differences between plain and complex bacterial flagellar filaments. *Journal of Molecular Biology*, 190, 569–576.
- Van Way, S.M., Hosking, E.R., Braun, T.F. & Manson, M.D. (2000) Mot protein assembly into the bacterial flagellum: a model based on mutational analysis of the *motB* gene. *Journal of Molecular Biology*, 297, 7–24.
- Wadhwa, N. & Berg, H.C. (2021) Bacterial motility: machinery and mechanisms. *Nature Reviews Microbiology*, 20(3), 1–13.
- Zatakia, H.M., Arapov, T.D., Meier, V.M. & Scharf, B.E. (2018) Cellular stoichiometry of methyl-accepting chemotaxis proteins in *Sinorhizobium meliloti*. *Journal of Bacteriology*, 200, e00614-00617.
- Zhu, S., Kumar, A., Kojima, S. & Homma, M. (2015) FliL associates with the stator to support torque generation of the sodium-driven polar flagellar motor of *Vibrio*. *Molecular Microbiology*, 98, 101–110.
- Zhu, S., Takao, M., Li, N., Sakuma, M., Nishino, Y., Homma, M. et al. (2014) Conformational change in the periplasmic region of the flagellar stator coupled with the assembly around the rotor. *Proceedings of the National Academy of Sciences*, 111, 13523–13528.

## SUPPORTING INFORMATION

Additional supporting information can be found online in the Supporting Information section at the end of this article.

**How to cite this article:** Sobe, R. C., Gilbert, C., Vo, L., Alexandre, G. & Scharf, B. E. (2022). FliL and its paralog MotF have distinct roles in the stator activity of the *Sinorhizobium meliloti* flagellar motor. *Molecular Microbiology*, 118, 223–243. <https://doi.org/10.1111/mmi.14964>